

Ultrafast Dynamics in Aprotic Molecular Liquids: A Femtosecond Raman-Induced Kerr Effect Spectroscopic Study

Hideaki Shirota,* Tomotsumi Fujisawa, Hiroki Fukazawa, and Keiko Nishikawa

Department of Nanomaterial Science, Graduate School of Advanced Integration Science, Chiba University, 1-33 Yayoi, Inage-ku, Chiba 263-8522

Received April 24, 2009; E-mail: shirota@faculty.chiba-u.jp

We have studied the ultrafast dynamics of forty aprotic molecular liquids by femtosecond optical heterodyne-detected Raman-induced Kerr effect spectroscopy. Some physical properties such as shear viscosity, density, and surface tension of the molecular liquids have also been measured. From the Fourier transform Kerr spectra in the frequency range of about 0–200 cm^{-1}, we have found that the first moment of the low-frequency intermolecular vibrational spectrum is moderately correlated with the root of the value of surface tension divided by density. This fact indicates that the microscopic intermolecular interaction is related to the macroscopic physical property of intermolecular force in molecular liquids. On the other hand, a correlation between the first moment of the intermolecular vibrational spectrum and the interaction energy of two identical molecules is almost nonexistent. The difference between the two relations suggests that the many-body interaction effect takes a hand in the intermolecular vibrational dynamics in molecular liquids. We have also found that the shapes of the broad low-frequency vibrational spectra for aromatic molecular liquids show a clearer bimodal feature than those for non-aromatic molecular liquids. Picosecond Kerr transients for most of the molecular liquids are non-exponential. The slowest relaxation time is qualitatively explained by the Stokes–Einstein–Debye model.

Because of its important roles in many chemical reactions, dynamics of molecular liquids is of long-standing interest in chemistry. For example, rapid collective fluctuation between a solute and solvents may predominantly affect barrier-crossing processes for chemical reactions and biological systems in solution, e.g., electron transfer, proton transfer, and protein folding. Therefore, studies of solvent dynamics around a solute are essential for detailed understanding of barrier-crossing processes in solutions.[1–9] On the basis of this scientific interest, experimental, simulation, and theoretical studies have been made to characterize and understand details of solvent reorganization processes in solutions. Maroncelli and co-workers summarized the femtosecond to picosecond solvation dynamics data of as many as 24 typical organic solvents measured by dynamic fluorescence Stokes shift of a solvatochromic probe, coumarin 153, in solutions.[10] Following this work, they also reported solvation dynamics data of coumarin 153 in six non-dipolar solvents.[11]

On the other hand, there have been fewer reports on ultrafast dynamics in pure liquids than those on solvation dynamics in solutions. This is probably because a specific interaction between solute and solvent is a main interest in chemistry: the solute–solvent interaction has a key role for barrier-crossing processes in solution, as mentioned above. However, understanding and characterizing ultrafast dynamics including intermolecular and intramolecular vibrational dynamics and molecular reorientation in pure liquids themselves are also essential for chemical physics, physical chemistry, and molecular science. We also believe that comparisons of dynamics between pure liquids and solutions provide clearer and deeper molecular-level understandings of molecular dynamics and reveal key roles of solute–solvent interaction and motions on reaction dynamics in solutions.[12,13]

Femtosecond optical heterodyne-detected Raman-induced Kerr effect spectroscopy (OHD-RIKES) is a powerful spectroscopic technique to observe the ultrafast molecular dynamics of transparent liquids, solutions, and solids.[14–20] Under conventional polarization, OHD-RIKES measures the depolarized Raman signal. Because high quality low-frequency spectra from about 0.3–300 cm^{-1} is usually available from the Kerr transient, this spectroscopy is very useful for investigating intermolecular vibrational dynamics and intermolecular interactions in condensed phases. Most of the earlier femtosecond OHD-RIKES studies were for understanding intermolecular vibrational dynamics and reorientation of pure liquids.[14–19] Currently, femtosecond OHD-RIKES is also applied for studying intermolecular vibrational dynamics, reorientation, and microscopic intermolecular interactions in complex condensed phases such as polymer liquids[21,22] and solutions,[23–27] microemulsions,[27–29] solvents in nanoporous glasses,[30,31] aqueous protein films[32] and solutions,[33–35] room-temperature ionic liquids,[36–38] and supercritical fluids.[39] An excellent review article in this field was written by Meech and co-workers recently.[40] Besides the above studies of ultrafast dynamics in simple and complex condensed phases, femtosecond RIKES is now applied to new spectroscopic techniques such as resonant pump Kerr effect spectroscopies[41–44] to investigate the solvent response around a solute (both solvation dynamics and chemical reactions).

Despite earlier studies, several questions regarding the intermolecular vibrational spectrum in molecular liquids still remain. (i) What is the general nature of the intermolecular

Published on the web November 10, 2009; doi:10.1246/bcsj.82.1347

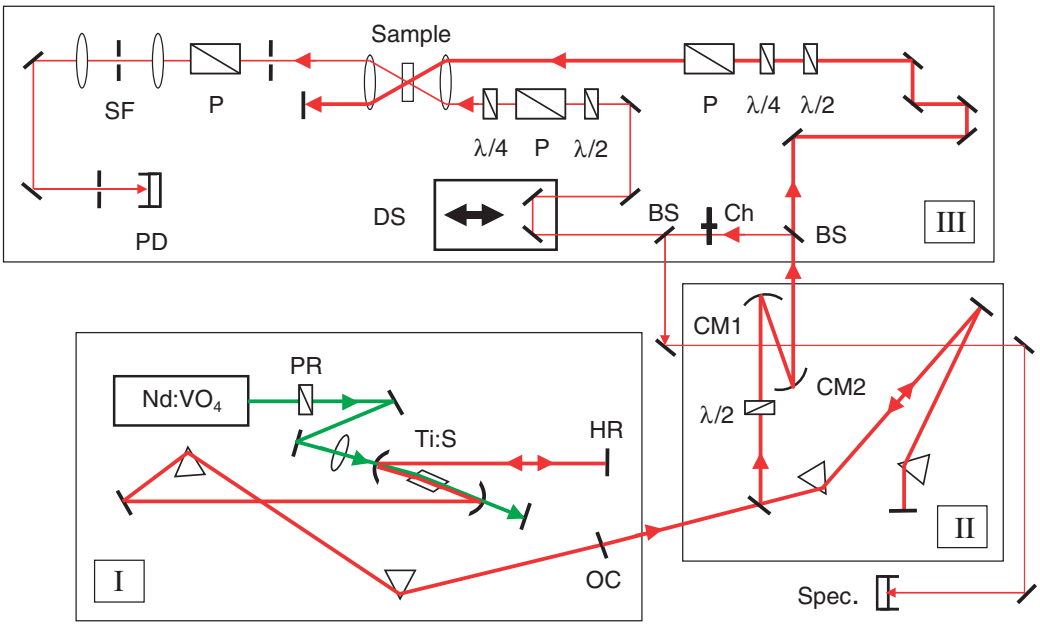

Figure 1. Schematic diagram of femtosecond OHD-RIKES used in this study. Section I, II, and III denote the light source (titanium:sapphire laser), group velocity dispersion control, and RIKES spectroscope, respectively. PR: polarizer rotator, Ti:S: titanium:sapphire crystal, HR: high reflector, OC: output coupler, $\lambda/2$: half wave plate, $\lambda/4$: quarter wave plate, CM: concave mirror, BS: beam splitter, Ch: chopper, DS: delay stage, P: polarizer, Spec.: spectrometer for monitor of laser spectrum, SF: spacial filter, and PD: photodiode.

vibrational spectrum in molecular liquids? (ii) What are the important factors for the characteristic frequency and shape of the intermolecular vibrational spectrum? (iii) Is there any correlation between the intermolecular vibrational spectrum and bulk properties? (iv) If there is, what properties? In this study, we have tackled these by the measurement of the ultrafast dynamics of forty simple molecular liquids by means of femtosecond OHD-RIKES. Twenty molecular liquids are non-aromatic and the other twenty are aromatic. About half of the molecular liquids measured in this study have already been reported by several groups including us,[12,45–83] but the data here are high quality and well-resolved in the wide frequency range of 0.2–750 cm^{-1}, which has rarely been reported. The reason why we have picked only aprotic molecular liquids in this study is that complex interactions such as hydrogen and ionic bonds create difficulties in understanding the intermolecular vibrational spectra of molecular liquids. Our main purposes in this study are: (i) overview and gaining an overall understanding of intermolecular vibration and reorientation in simple aprotic molecular liquids, (ii) comparing the intermolecular vibration band with bulk properties, and (iii) making a comprehensive database for intermolecular vibrations and reorientations of aprotic molecular liquids.

Experimental and Quantum Chemistry Calculation Methods

Experiments. Femtosecond OHD-RIKES used in this study is based on a standard design established by McMorrow, Lotshaw, and co-workers.[15,47] The scheme of the OHD-RIKES used in our laboratory is shown in Figure 1.[22,59] The light source was a lab-built titanium:sapphire laser that was based on a laser kit (CDP Corp., TISSA-kit 20) pumped by about 3.4 W of 532 nm light from a Nd:VO_4 diode laser (Spectra Physics, Millennia Pro 5sJ) (Figure 1 section I). The center wavelength of the titanium: sapphire laser was about 805 nm with a width of about 75 nm full width at half maximum (FWHM). The repetition rate was about 85 MHz, and the output power was 300–320 mW. At first, the laser beam was routed to an optical line consisting of a pair of fused silica Brewster prisms to make a group velocity dispersion control for the OHD-RIKES spectrometer, as shown in Figure 1 section II. The distance between the prisms was as long as 2.04 m. The light polarization was rotated to vertical by a half-wave plate, and then the light was collimated by two concave mirrors with the focusing points of 200 and 50 mm. After the group velocity dispersion control part, the laser beam goes into the OHD-RIKES spectrometer part (section III in Figure 1). The beam was separated into pump and probe beams with an intensity ratio of about 95:5 by an uncoated fused silica interferometric wedge. The pump beam was then routed through a half-wave plate, a quarter-wave plate, and a Glan–Thompson polarizer set to transmit vertically polarized light. The pump beam intensity was modulated by a mechanical chopper at 1 kHz (Stanford Research Systems, SR540). The probe beam was routed through an uncoated fused silica interferometric wedge, a variable optical delay line (Sigma Tech, FS-1050, 0.2 μm accuracy), a half-wave plate, a Glan–Thompson polarizer to set the polarization of +45° from vertical, and a quarter-wave plate. The pump and probe beams were focused on the sample with a 150 mm focal length achromatic lens and recollimated with an identical lens. The pump beam was blocked, the probe beam was sent through a second Glan–Thompson polarizer, which was set at the polarization of −45° from vertical, and a spatial filter consisting of two achromatic lenses on both the sides of a 250 μm pinhole. To achieve heterodyne detection, an out of phase local oscillator was introduced by rotating the input polarizer by either ca. +1.5 or ca. –1.5° away from the homodyne orientation (extinction). To avoid any homodyne contribution, the measurements of both ca.

+1.5 or ca. –1.5° probe input polarizations were employed by monitoring the intensity of the local oscillator. The Kerr signal was detected by a large area amplified PIN photodiode (New Focus, 2032) and recorded by a lock-in amplifier (Stanford Research Systems, SR830). The laser pulse cross-correlation in this OHD-RIKES setup measured with a 200 μm potassium dihydrogen phosphate (KDP) type-I crystal placed in the sample cell position was 31 ± 3 fs (FWHM) (equivalent to a 20 ± 2 fs assuming a sech^2 pulse shape). Typical scan conditions are 0.5 μm/step for a high time resolution transients and 3.0 or 5.0 μm/step for long time window data. The long time window data were measured for at least twice as long as the slowest relaxation time. All the experiments were made at 297 ± 1 K.

All the aprotic molecular liquids were commercially available from Tokyo Kasei, Wako Pure Chemical, Kanto Chemicals, or Aldrich and used from an unopened bottle without further purification. The sample molecular liquids were injected into a quartz cell (Tosoh Quartz) with an optical path length of 3 mm via 0.2- and 0.02-μm Anotop filters (Whatman) for femtosecond OHD-RIKES measurements.

Densities of the molecular liquids were measured with a density meter (Anton Paar, DMA 4500) at 297.0 ± 0.1 K. A reciprocating electromagnetic piston viscometer (Cambridge Viscosity, ViscoLab 4100) with a circulating water bath (Yamato, BB300) was used for the shear viscosity measurements at 297.0 ± 0.2 K. Surface tensions of the samples were measured by a du Noüy tensiometer (Yoshida Seisakusho) at 296.7 ± 0.5 K.

Quantum Chemistry Calculations. Ab initio quantum chemistry calculations based on the density functional theory at B3LYP/aug-cc-pVDZ level[84–87] were performed for all forty molecules to obtain the optimized structures and polarizability tensor elements by the Gaussian 03 program suite.[88] Atom coordinates for the stabilized molecules are summarized in Supporting Information. On the basis of the optimized structures of the molecules, the single point energies of the cation forms of the molecules were also calculated to estimate the ionization energies I. Using calculated polarizability tensor elements, the mean polarizabilities α_0, and polarizability anisotropies α_{anis} were estimated by the following equations:[89]

$$\alpha_0 = \frac{\alpha_{xx} + \alpha_{yy} + \alpha_{zz}}{3} \tag{1}$$

$$\alpha_{\mathrm{anis}} = \sqrt{\frac{(\alpha_{xx} - \alpha_{yy})^2 + (\alpha_{yy} - \alpha_{zz})^2 + (\alpha_{zz} - \alpha_{xx})^2 + 6(\alpha_{xy}{}^2 + \alpha_{yz}{}^2 + \alpha_{zx}{}^2)}{2}} \tag{2}$$

where α_{xx}, α_{yy}, α_{zz}, α_{xy}, α_{yz}, and α_{zx} are the polarizability tensor elements. Note that the quantum chemistry calculation for the B3LYP functional with the basis set of cc-pVDZ having augmented functions gives a better polarizability value than that without augmented functions.[90] I was calculated as,

$$I = E_0(\mathrm{cation}) - E_0(\mathrm{neutral}) \tag{3}$$

where E_0(neutral) is the energy of the target molecule in the neutral state and E_0(cation) is the energy of its cation form. Because the purpose in this study is a qualitative discussion on the intermolecular interaction in aprotic molecular liquids, the contribution of the zero-point vibrational energy is not taken into consideration. The molecular properties, dipole moment μ, α_0, α_{anis}, and I, are summarized in Table 1. These values will be used to estimate the intermolecular interaction energies for two identical molecules in the gas phase for comparison with the intermolecular vibrations in molecular liquids studied here. To find the dielectric effect of solvent medium, further calculation based on the density functional theory of B3LYP/aug-cc-pVDZ level with IEF-PCM for eight molecules (acetonitrile, dimethyl sulfoxide, carbon tetrachloride, chloroform, dichloromethane, benzene, chlorobenzene, and toluene, whose solvent parameters are available as default in the Gaussian 03 program) was also made. μ, α_0, α_{anis}, and I including the dielectric medium effect are summarized in Supporting Information.

Data Analysis. Standard Fourier transform analysis established by McMorrow and Lotshaw[47,91] was made for the measured Kerr transients. To obtain a sufficient number of data points for a spectrum with a reasonable accuracy, it is necessary to extend the high time resolution data over a longer time range than that has been experimentally recorded. To achieve this, the longer time scale Kerr transients recorded with lower time resolution were analyzed by a multi-exponential function ($\sum_i a_i \exp(-t/\tau_i)$). The fits to the long Kerr transients were made from 3.0 ps. Figure 2a shows a bi-exponential function fit to the long-time Kerr transient of benzene, as an example. The residuals are also shown in Figure 2. The quality of the fit for all the data are similar to that for benzene, except for some low signal intensity samples such as 1,4-dioxane, tetrahydrofuran, and acetone. Fit parameters for all the samples are summarized in Table 2. Besides a multi-exponential function, a practical function based on mode coupling theory (MCT) is also often used.[92–94] The function is given by,

$$f_{\mathrm{MCT}}(t) = (pt^{-z} + dt^{b-1}) \exp(-t/\tau_\alpha) \tag{4}$$

where the term pt^{-z} is known as the intermediate power law, the term dt^{b-1} is known as the von Schweidler power law, which expresses the crossover between β and α relaxations, and τ_α is the characteristic time of the α relaxation. Figure 2b shows a fit by a MCT function to the long-time Kerr transient of benzene. As seen in Figures 2a and 2b, the quality of the fit by a MCT function is quite competitive to that by a bi-exponential function. However, the fit by a MCT function is not stable and the parameters include large standard deviations in comparison with a bi-exponential function (bi-exponential fit: $a_1 = 0.0812 \pm 0.0139$, $\tau_1 = 0.858 \pm 0.058$ ps, $a_2 = 0.0468 \pm 0.0008$, and $\tau_2 = 2.835 \pm 0.017$ ps; MCT fit: $p = 0.0327 \pm 0.0421$, $z = 1.659 \pm 5.61$, $d = 0.0558 \pm 0.0891$, $b = 0.756 \pm 0.765$, and $\tau_a = 3.172 \pm 0.478$ ps). Therefore, we have used a multi-exponential function for fits to the Kerr transients for all the molecular liquids. All the Kerr trajectories and their multi-exponential function fits for the forty aprotic molecular liquids are summarized in Supporting Information.

Prior to Fourier transform analysis, the data set was extended to 131072 points by the fit function with a time step of 3.3355 fs, yielding spectra with about 0.07624 cm^{-1}/point spacing. All the Kerr spectra obtained in this study are well resolved up to about 750 cm^{-1}. As mentioned before, about half the numbers of molecular liquids studied here have already been reported, and the low-frequency broad spectra measured in this study are similar to those reported.[12,45–83] The Kerr spectra of the forty aprotic molecular liquids are available in Supporting Information. Before the line shape analysis of the low-frequency spectrum (<150 cm^{-1}), the Fourier transform of the picosecond reorientation response was subtracted from the spectrum to emphasize the higher frequency intermolecular vibration components, as shown in Figure 3.

The spectral shape of the low-frequency broad Kerr spectrum of benzene is complex, unlike intramolecular vibrational modes. Traditionally, the broad Kerr spectra of simple molecular liquids have been analyzed by either a Bucaro–Litovits function (or

Table 1. Formula Weight FW, Shear Viscosities η, Surface Tension γ, Density d, Molar Volume V_d, Molar Radius r_d, van der Waals Volume V_{VDW}, Mean Polarizability α_0, Polarizability Anisotropy α_{anis}, and Ionization Energy I[a)]

	FW /g mol^{-1}	η /cP	γ /mN m^{-1}	d /g mL^{-1}	V_d /Å^3	r_d /Å	V_{VDW} /Å^3	μ /Debye	α_0 /Å^3	α_{anis} /Å^3	I /eV
A. Non-aromatic liquids											
Acetonitrile	41.05	0.378	28.9	0.7777	87.68	2.756	47.1	4.054	4.437	2.462	12.195
Propionitrile	55.08	0.418	26.5	0.7778	117.63	3.040	64.1	4.165	6.295	2.716	11.754
Dimethyl sulfoxide	78.13	1.973	43.0	1.0963	118.38	3.046	72.2	4.317	8.252	2.733	8.851
N,*N*-Dimethylformamide	73.09	0.800	36.4	0.9448	128.46	3.130	77.7	4.154	7.891	3.223	9.230
Carbon disulfide	76.14	0.363	32.4	1.2571	100.61	2.885	51.8	0.000	8.121	8.666	10.123
Propylene carbonate	102.09	2.424	42.0	1.2006	140.66	3.226	82.8	5.759	8.688	2.134	10.835
Methyl acetate	74.08	0.380	24.3	0.9286	132.52	3.163	71.0	1.927	6.990	2.483	10.377
Ethyl acetate	88.11	0.439	23.6	0.8957	163.41	3.392	88.0	2.112	8.900	3.199	10.191
Acetone	58.08	0.318	23.0	0.7861	122.73	3.083	64.8	3.107	6.395	1.917	9.461
2-Butanone	72.11	0.397	24.1	0.8012	149.51	3.293	81.8	2.959	8.172	2.468	9.383
3-Pentanone	86.13	0.446	24.8	0.8105	176.53	3.480	98.8	2.821	9.953	3.182	9.301
Tetrahydrofuran	72.11	0.459	26.9	0.8831	135.64	3.187	74.2	1.825	7.852	1.658	9.268
1,4-Dioxane	88.11	1.153	33.2	1.0292	142.21	3.238	80.4	0.000	8.643	1.728	9.047
Carbon tetrachloride	153.82	0.866	27.2	1.5863	161.08	3.375	84.8	0.000	10.393	0.000	11.095
Chloroform	119.38	0.512	27.3	1.4714	134.77	3.181	70.7	1.112	8.391	2.864	11.069
Dichloromethane	84.93	0.416	28.0	1.3153	107.26	2.947	56.6	1.721	6.354	2.917	11.303
Dibromomethane	173.83	0.936	40.5	2.4843	116.23	3.027	66.0	1.529	8.487	4.526	10.399
Bromochloromethane	129.38	0.636	32.9	1.9222	111.81	2.989	61.3	1.628	7.403	3.688	10.778
1,2-Dichloroethane	98.96	0.751	32.7	1.2472	131.80	3.157	73.6	0.000	8.417	5.056	10.876
1,2-Dibromoethane	187.86	1.516	40.3	2.1711	143.73	3.250	83.0	0.000	10.882	7.295	10.161
B. Aromatic liquids											
Benzene	78.11	0.591	28.9	0.8747	148.34	3.284	80.4	0.000	10.402	5.583	9.237
Fluorobenzene	96.10	0.563	27.8	1.0201	156.49	3.343	85.0	1.623	10.391	5.804	9.247
Hexafluorobenzene	186.05	0.914	22.2	1.6090	192.07	3.579	108.0	0.000	10.790	6.928	10.050
Chlorobenzene	112.56	0.717	33.4	1.1022	169.65	3.434	94.9	1.839	12.582	7.923	9.025
Bromobenzene	157.01	1.030	36.7	1.4876	175.33	3.472	99.6	1.860	13.763	8.966	8.894
Toluene	92.14	0.555	28.5	0.8631	177.33	3.485	97.8	0.406	12.462	6.838	8.773
(Trifluoromethyl)benzene	146.11	0.610	23.9	1.1830	205.16	3.659	110.4	3.025	12.457	6.481	9.790
Ethylbenzene	106.17	0.624	28.6	0.8639	204.14	3.653	114.8	0.409	14.388	7.092	8.713
n-Propylbenzene	120.19	0.808	28.3	0.8597	232.25	3.813	131.8	0.436	16.375	8.346	8.642
Cumene	120.19	0.740	28.0	0.8582	232.64	3.815	131.8	0.400	16.206	7.105	8.665
n-Butylbenzene	134.22	0.975	28.5	0.8572	260.10	3.960	148.8	0.491	18.313	8.649	8.597
Anisole	108.14	1.028	35.2	0.9901	181.42	3.512	104.0	1.306	13.337	7.792	8.206
N,*N*-Dimethylaniline	121.18	1.267	36.7	0.9528	211.28	3.695	127.7	2.004	16.459	9.615	7.178
Benzonitrile	103.12	1.257	39.0	1.0014	171.06	3.444	99.5	4.732	13.049	9.601	9.590
o-Xylene	106.17	0.777	30.0	0.8764	201.23	3.635	115.2	0.679	14.417	7.701	8.502
m-Xylene	106.17	0.605	28.8	0.8607	204.91	3.657	115.2	0.320	14.528	7.943	8.469
p-Xylene	106.17	0.612	28.2	0.8575	205.67	3.662	115.2	0.078	14.573	8.609	8.376
Mesitylene	120.19	0.668	28.9	0.8619	231.63	3.810	132.6	0.031	16.610	8.698	8.362
1-Methylimidazole	82.10	1.600	44.9	1.0318	132.18	3.160	78.7	4.165	9.314	4.280	8.694
1-Butylimidazole	124.18	3.369	34.8	0.9481	217.58	3.731	129.7	4.524	14.974	5.983	8.510

a) Values for η, γ, and d are at 297 K.

an Ohmic (eq 5)),[95,96] a sum of Ohmic and anti-symmetrized Gaussian (eq 6) functions,[48,52,54,56–58,97–99] or a function based on the multi-mode Brownian oscillator model (eq 7).[49,76,100]

$$I_O(\omega) = \sum_i a_{Oi}\omega \exp(-\omega/\omega_{Oi}) \tag{5}$$

$$I_G(\omega) = \sum_i \left\{ a_{Gi} \exp\left[\frac{-2(\omega-\omega_{Gi})^2}{\Delta\omega_{Gi}{}^2}\right] - a_{Gi} \exp\left[\frac{-2(\omega+\omega_{Gi})^2}{\Delta\omega_{Gi}{}^2}\right]\right\} \tag{6}$$

$$I_{BO}(\omega) = \sum_i \frac{a_{BOi}\gamma_{BOi}\omega}{(\omega_{BOi}{}^2-\omega^2)^2+\gamma_{BOi}{}^2\omega^2} \tag{7}$$

where a_{Oi} and ω_{Oi} are the amplitude and characteristic frequency parameters of the i-th Ohmic line shape, respectively, a_{Gi}, ω_{Gi}, and $\Delta\omega_{Gi}$ are the amplitude, characteristic frequency, and band width parameters for the i-th anti-symmetrized Gaussian function, respectively, and a_{BOi}, ω_{BOi}, and γ_{BOi} are the amplitude, frequency, and damping parameters for the i-th Brownian oscillator, respectively. If a clear intramolecular vibrational band locates in a low-frequency region (ca. 150 cm^{-1} in a typical case), a Lorentzian

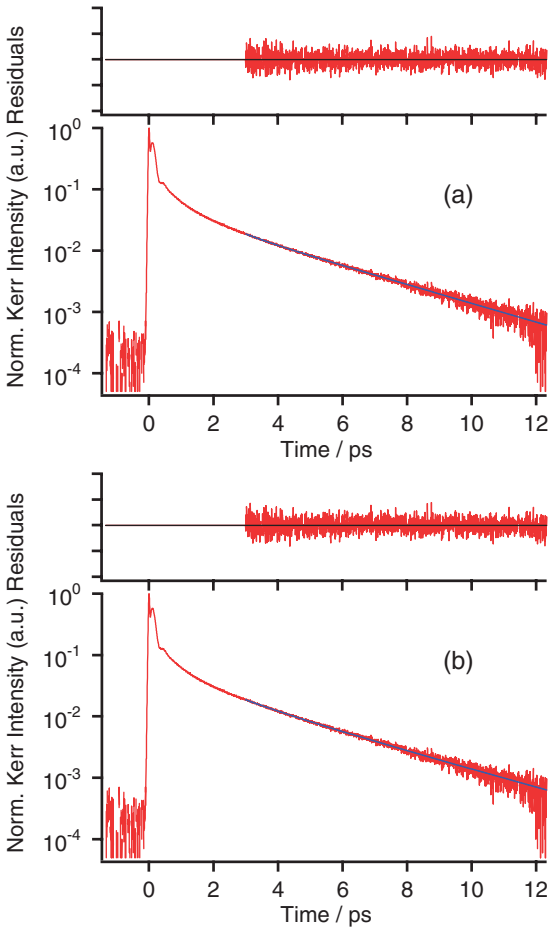

Figure 2. Kerr transient for benzene (red transient in lower figure) and its fits by (a) a biexponential function and (b) a practical function based on the mode coupling theory (blue line in lower figure). The residuals (red trajectories in upper figures for the Kerr transient figures) are also shown.

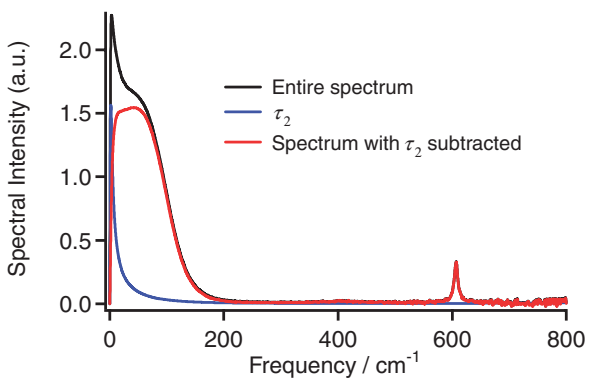

Figure 3. Fourier transform Kerr spectra for benzene. Black, blue, and red lines denote the spectrum including all the contributions, the contribution of picosecond reorientation (τ_2), and the spectrum subtracted the contribution of picosecond reorientation (intermolecular vibration), respectively.

function is added to fit the intramolecular vibrational band. Both the Bucaro–Litovitz (or Ohmic) and anti-symmetrized Gaussian functions are empirically used, and a sum of these functions well fits broad Kerr spectra of not only simple molecular

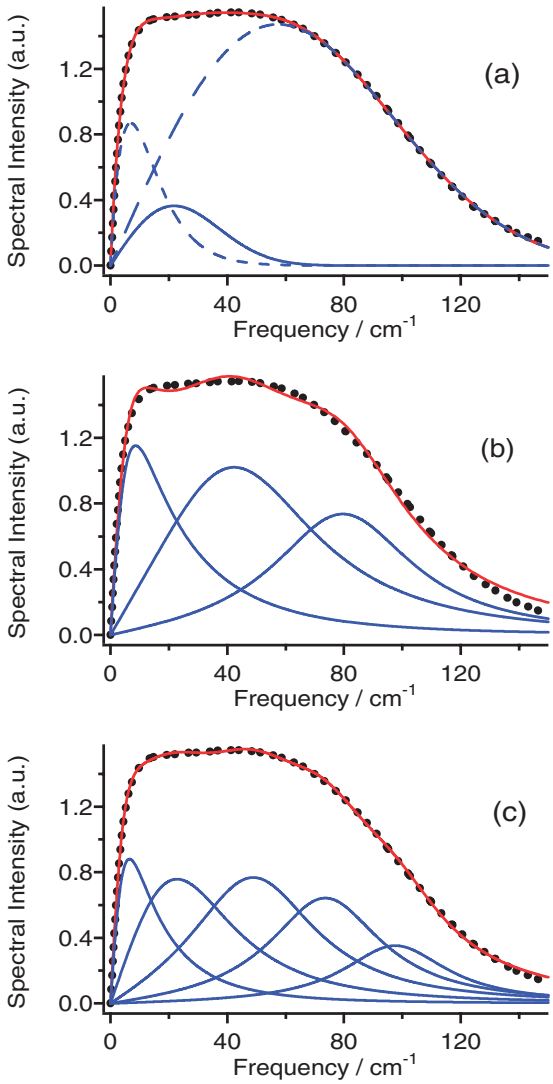

Figure 4. Spectral fits to the broad low-frequency Kerr spectrum for benzene by (a) sum of an Ohmic (short dashed line) and anti-symmetrized Gaussian functions (solid and long dashed lines) (eqs 5 and 6) and multi-mode Brownian oscillator model (eq 7) of (b) three Brownian oscillators and (c) five Brownian oscillators.

liquids[48,52,54,56–58,97–99] but also complex condensed phases such as polymer solutions and liquids,[22,24–27] microemulsions,[27–29] and room-temperature ionic liquids.[37,38,101–104] On the other hand, the Brownian oscillator model treats the time-dependent fluctuation of solvent molecules as harmonic oscillators.[49,76,100,105–107]

Figure 4 compares the spectral fits by (a) a sum of an Ohmic line-shape function and two anti-symmetrized Gaussian functions, (b) three Brownian oscillators, and (c) five Brownian oscillators for benzene, as an example. As clearly shown in Figure 4, a sum of an Ohmic function and two anti-symmetrized Gaussian functions gives a better fit for the Kerr spectrum of benzene than a sum of three Brownian oscillators. To obtain a satisfactory fit by the multi-mode Brownian oscillator model, at least two more Brownian oscillators are necessary for the spectrum of benzene, as found in Figure 4. We have therefore used a sum of Ohmic and anti-symmetrized Gaussian functions to represent the low-frequency Kerr spectra for the forty aprotic molecular liquids in this study.

Table 2. Fit Parameters of Kerr Transients by a Multi-Exponential Function[a)]

	a_1 ($a_1/\Sigma a_n$)	τ_1/ps	a_2 ($a_2/\Sigma a_n$)	τ_2/ps	a_3 ($a_3/\Sigma a_n$)	τ_3/ps
A. Non-aromatic liquids						
Acetonitrile	0.0756 (0.751)	1.32	0.0250 (0.249)	1.98		
Propionitrile	0.0315 (0.543)	1.71	0.0265 (0.457)	2.89		
Dimethyl sulfoxide	0.0086 (0.775)	0.97	0.0025 (0.225)	6.82		
N,*N*-Dimethylformamide	0.0278 (0.507)	1.53	0.0270 (0.493)	5.06		
Carbon disulfide	0.3337 (0.567)	0.49	0.2551 (0.433)	1.71		
Propylene carbonate	0.0119 (0.543)	2.59	0.0100 (0.457)	15.13		
Methyl acetate	0.0324 (0.559)	0.86	0.0256 (0.441)	2.89		
Ethyl acetate	0.0436 (0.741)	0.88	0.0152 (0.259)	4.67		
Acetone	0.0268 (1.000)	1.21				
2-Butanone	0.0544 (0.673)	0.70	0.0126 (0.327)	2.15		
3-Pentanone	0.0103 (0.592)	1.56	0.0071 (0.308)	4.01		
Tetrahydrofuran	0.0020 (1.000)	1.87				
1,4-Dioxane	0.0095 (0.673)	1.09	0.0041 (0.327)	3.00		
Carbon tetrachloride	—	—	—	—		
Chloroform	0.0067 (0.247)	1.07	0.0204 (0.753)	2.81		
Dichloromethane	0.1313 (0.750)	0.51	0.0438 (0.250)	2.13		
Dibromomethane	0.0135 (0.408)	3.16	0.0140 (0.592)	6.28		
Bromochloromethane	0.0262 (0.663)	2.49	0.0133 (0.337)	4.24		
1,2-Dichloroethane	0.0154 (0.440)	1.65	0.0196 (0.560)	6.48		
1,2-Dibromoethane	0.0135 (0.453)	2.16	0.0163 (0.547)	19.06		
B. Aromatic liquids						
Benzene	0.0812 (0.634)	0.86	0.0468 (0.366)	2.84		
Fluorobenzene	0.0595 (0.467)	1.11	0.0680 (0.533)	3.94		
Hexafluorobenzene	0.0794 (0.327)	2.19	0.1028 (0.673)	13.23		
Chlorobenzene	0.0429 (0.429)	1.65	0.0572 (0.571)	7.05		
Bromobenzene	0.0299 (0.327)	2.07	0.0369 (0.673)	9.82		
Toluene	0.0403 (0.458)	1.41	0.0477 (0.542)	5.10		
(Trifluoromethyl)benzene	0.0708 (0.646)	1.87	0.0388 (0.354)	7.38		
Ethylbenzene	0.0416 (0.644)	1.84	0.0230 (0.356)	7.48		
n-Propylbenzene	0.0311 (0.679)	2.61	0.0147 (0.321)	12.03		
Cumene	0.0317 (0.679)	1.93	0.0179 (0.321)	7.88		
n-Butylbenzene	0.0237 (0.639)	2.95	0.0123 (0.361)	14.88		
Anisole	0.0287 (0.537)	2.31	0.0247 (0.463)	10.25		
N,*N*-Dimethylaniline	0.0149 (0.498)	2.49	0.0150 (0.502)	15.90		
Benzonitrile	0.0479 (0.453)	1.07	0.0159 (0.151)	4.96	0.0419 (0.396)	19.07
o-Xylene	0.0278 (0.470)	1.94	0.0313 (0.530)	9.74		
m-Xylene	0.0311 (0.422)	1.85	0.0426 (0.578)	7.47		
p-Xylene	0.0344 (0.422)	1.86	0.0390 (0.578)	10.46		
Mesitylene	0.0223 (0.397)	2.69	0.0339 (0.603)	10.88		
1-Methylimidazole	0.0155 (0.598)	2.26	0.0104 (0.402)	11.24		
1-Butylimidazole	0.0062 (0.453)	1.91	0.0030 (0.151)	7.81	0.0020 (0.396)	48.86

a) Fit from 3 ps.

The fit parameters for the forty molecular liquids are summarized in Table 3. The values of the first moments of broad low-frequency spectra M_1 ($M_1 = \int \omega I(\omega) \mathrm{d}\omega / \int I(\omega) \mathrm{d}\omega$) for the forty aprotic molecular liquids are also summarized in Table 3. Fit curves for the low-frequency broad Kerr spectra of all forty molecular liquids are available in Supporting Information.

Results and Discussion

Physical Properties: Shear Viscosity, Density, Surface Tension, and Molecular Volumes. Data of shear viscosity η, density d, and surface tension γ at 297 K for the forty aprotic molecular liquids are summarized in Table 1. η, d, and γ at 298 K for most of the molecular liquids measured in this study can be found in the CRC Handbook,[108] and the values at 297 K in this study are similar to the values at 298 K in the CRC Handbook except for the values of η for propionitrile and hexafluorobenzene. The data, which are inconsistent with the values tabulated in the CRC Handbook, have been checked in other literature,[109–111] and we have confirmed that the data measured here are similar to the reported values. These data will be referenced to the time-resolved data in the following subsections, because these physical properties are related to the dynamic properties in molecular liquids.

Table 3. Fit Parameters of Fourier Transform Kerr Spectra for Simple Molecular Liquids

	M_1[a] /cm^{-1}	a_{O1} (A_{O1}[b])	ω_{O1} /cm^{-1}	a_{O2} (A_{O2}[b])	ω_{O2} /cm^{-1}	a_{O3} (A_{O3}[b])	ω_{O3} /cm^{-1}	a_{G1} (A_{G1}[b])	ω_{G1} /cm^{-1}	$\Delta\omega_{G1}$ /cm^{-1}	a_{G2} (A_{G2}[b])	ω_{G2} /cm^{-1}	$\Delta\omega_{G2}$ /cm^{-1}	a_{L1}	ω_{L1} /cm^{-1}	$\Delta\omega_{L1}$ /cm^{-1}	a_{L2}	ω_{L2} /cm^{-1}	$\Delta\omega_{L2}$ /cm^{-1}
A. Non-aromatic liquids																			
Acetonitrile	60.2	0.810 (0.055)	3.4	0.251 (0.179)	11.0			1.738 (0.492)	25.3	92.0	1.032 (0.274)	23.0	149.5						
Propionitrile	54.4	0.529 (0.049)	2.8	0.143 (0.181)	10.3			1.157 (0.544)	20.8	82.6	0.645 (0.226)	14.9	147.6						
Dimethyl sulfoxide	63.5	0.0390 (0.031)	4.1	0.017 (0.153)	13.9			0.215 (0.816)	44.7	102.1									
N,*N*-Dimethylformamide	61.8	0.0290 (0.040)	3.3	0.101 (0.225)	13.4			0.951 (0.602)	27.3	91.9	0.163 (0.133)	33.9	221.7						
Carbon disulfide	41.7	0.378 (0.264)	11.5					1.627 (0.436)	35.0	46.3	0.749 (0.300)	51.8	70.1						
Propylene carbonate	66.8	0.391 (0.017)	1.6	0.127 (0.053)	5.1	0.052 (0.297)	18.8	0.456 (0.502)	37.9	94.2	0.118 (0.131)	35.0	266.4						
Methyl acetate	58.2	0.132 (0.103)	7.6	0.030 (0.336)	28.9			0.884 (0.479)	30.8	83.8	0.076 (0.082)	40.7	207.9						
Ethyl acetate	52.0	0.134 (0.065)	5.0	0.051 (0.243)	15.5			0.432 (0.414)	26.2	75.1	0.207 (0.278)	35.9	123.7	21.0	134.2	23.4	18.1	209.2	31.3
Acetone	60.2	0.066 (0.160)	11.7					0.665 (0.529)	23.5	81.1	0.340 (0.311)	26.2	140.7						
2-Butanone	54.8	0.086 (0.070)	6.1	0.028 (0.369)	24.2			0.398 (0.440)	26.5	84.5	0.133 (0.121)	20.8	146.8						
3-Pentanone	54.9	0.107 (0.031)	3.5	0.055 (0.147)	10.7			0.479 (0.543)	26.2	71.8	0.182 (0.279)	33.8	137.1						
Tetrahydrofuran	53.5	0.035 (0.189)	10.4					0.252 (0.437)	18.7	69.0	0.116 (0.374)	35.1	120.0						
1,4-Dioxane	52.1	0.045 (0.038)	4.0	0.023 (0.187)	12.3			0.192 (0.775)	46.9	78.1									
Carbon tetrachloride	39.0	0.037 (0.107)	5.2					0.218 (0.569)	13.0	48.3	0.050 (0.324)	33.5	89.2	28.6	218.1	4.9			
Chloroform	39.2	0.138 (0.171)	7.9					1.020 (0.611)	15.8	56.6	0.532 (0.218)	10.3	99.3						
Dichloromethane	46.5	0.114 (0.158)	9.2					1.088 (0.552)	16.2	60.6	0.415 (0.290)	21.8	116.3						
Dibromomethane	36.4	0.600 (0.033)	1.5	0.192 (0.163)	5.9			0.953 (0.594)	13.5	46.8	0.227 (0.210)	19.3	119.0	9.1	172.8	3.6			
Bromochloromethane	38.9	0.738 (0.051)	2.0	0.182 (0.214)	8.1			0.920 (0.463)	14.8	53.9	0.389 (0.272)	19.9	107.9						
1,2-Dichloroethane	46.5	0.184 (0.027)	2.6	0.089 (0.134)	8.2			0.512 (0.530)	27.0	55.9	0.366 (0.309)	19.3	115.0	15.5	125.9	12.6			
1,2-Dibromoethane	33.3	0.260 (0.025)	1.8	0.132 (0.140)	13.5			0.870 (0.697)	13.5	47.1	0.104 (0.138)	21.7	112.0	9.0	84.8	13.7			

Continued on next page.

Continued.

	M_1[a] /cm^{-1}	a_{O1} (A_{O1}[b])	ω_{O1} /cm^{-1}	a_{O2} (A_{O2}[b])	ω_{O2} /cm^{-1}	a_{O3} (A_{O3}[b])	ω_{O3} /cm^{-1}	a_{G1} (A_{G1}[b])	ω_{G1} /cm^{-1}	$\Delta\omega_{G1}$ /cm^{-1}	a_{G2} (A_{G2}[b])	ω_{G2} /cm^{-1}	$\Delta\omega_{G2}$ /cm^{-1}	a_{L1}	ω_{L1} /cm^{-1}	$\Delta\omega_{L1}$ /cm^{-1}	a_{L2}	ω_{L2} /cm^{-1}	$\Delta\omega_{L2}$ /cm^{-1}
B. Aromatic liquids																				
Benzene	58.5	0.340 (0.104)	6.9					0.387 (0.079)	19.7	33.9	1.518 (0.817)	54.3	83.6							
Fluorobenzene	53.1	0.238 (0.035)	4.6	0.222 (0.090)	7.6			0.582 (0.105)	14.2	38.6	1.391 (0.770)	52.6	76.1							
Hexafluorobenzene	33.7	1.826 (0.045)	1.9	0.785 (0.202)	6.2			1.194 (0.193)	13.4	34.5	1.488 (0.560)	43.8	48.6							
Chlorobenzene	50.9	0.475 (0.025)	2.6	0.288 (0.139)	7.9			0.654 (0.124)	12.8	44.6	1.150 (0.712)	52.5	76.2							
Bromobenzene	48.9	0.528 (0.023)	2.0	0.299 (0.135)	6.7			0.868 (0.220)	13.3	40.4	0.768 (0.622)	61.1	68.4							
Toluene	55.0	0.298 (0.025)	3.2	0.220 (0.103)	7.5			0.393 (0.069)	11.5	35.7	1.228 (0.803)	49.3	82.8							
(Trifluoromethyl)benzene	42.1	1.151 (0.044)	2.4	0.537 (0.214)	7.8			1.249 (0.184)	11.8	44.6	1.200 (0.558)	55.1	61.1	75.1	139.1	7.8				
Ethylbenzene	49.8	0.656 (0.039)	2.4	0.245 (0.158)	8.0			0.664 (0.107)	8.2	47.0	0.889 (0.696)	56.7	69.7	70.8	156.0	17.0				
n-Propylbenzene	52.0	1.044 (0.033)	1.7	0.289 (0.128)	6.3			0.743 (0.093)	5.7	38.2	0.872 (0.746)	45.2	86.9	174.2	122.1	34.1				
Cumene	48.1	0.510 (0.029)	2.2	0.238 (0.114)	6.4			0.591 (0.096)	7.1	35.0	0.878 (0.761)	48.4	70.3	56.8	141.6	11.1				
n-Butylbenzene	51.8	0.949 (0.029)	1.5	0.255 (0.116)	5.8			0.665 (0.092)	5.3	36.3	0.743 (0.763)	46.7	83.0	192.8	96.7	33.6				
Anisole	56.9	0.706 (0.022)	1.9	0.263 (0.114)	6.9			0.176 (0.047)	19.7	27.2	1.122 (0.817)	47.2	88.9							
N,*N*-Dimethylaniline	52.0	0.436 (0.023)	1.8	0.151 (0.137)	7.5			0.200 (0.106)	19.1	39.0	0.572 (0.734)	56.5	71.5	125.3	152.0	34.5				
Benzonitrile	52.2	1.679 (0.010)	0.9	0.539 (0.029)	2.6	0.249 (0.147)	8.7	0.611 (0.118)	12.8	50.3	1.154 (0.696)	61.8	65.1	28.8	157.6	14.6	20.0	173.0	7.4	
o-Xylene	51.4	0.448 (0.023)	2.2	0.219 (0.115)	7.0			0.311 (0.052)	8.1	32.4	1.104 (0.810)	39.7	82.9	24.8	179.9	11.3				
m-Xylene	52.2	0.466 (0.027)	2.3	0.220 (0.115)	7.0			0.310 (0.061)	9.7	34.7	1.078 (0.797)	39.7	85.7							
p-Xylene	52.5	0.534 (0.029)	2.4	0.228 (0.129)	7.7			0.267 (0.066)	14.0	40.6	1.033 (0.776)	53.7	73.1	34.3	155.5	25.4				
Mesitylene	50.6	0.766 (0.026)	1.6	0.228 (0.127)	6.5			0.145 (0.054)	18.1	27.9	1.003 (0.793)	32.9	87.5							
1-Methylimidazole	68.5	0.360 (0.015)	1.9	0.138 (0.085)	7.4			0.428 (0.105)	11.3	48.2	0.708 (0.795)	72.0	88.5	39.6	222.2	18.8				
1-Butylimidazole	69.5	0.853 (0.006)	0.6	0.212 (0.016)	2.1	0.067 (0.087)	8.5	0.700 (0.276)	11.3	66.3	0.448 (0.615)	91.0	62.0	50.2	172.8	30.2				

a) $M_1 = \int \omega I(\omega) d\omega / \int I(\omega) d\omega$. $I(\omega)$ is the lineshape for a sum of an Ohmic and two or three anti-symmetrized Gaussian functions obtained by the Kerr spectrum fit. The integration is made from 0 to 350 cm^{-1}. b) Values are normalized by spectral area. $A_i = \int I_i(\omega) d\omega / \int I(\omega) d\omega$.

The values of molecular properties such as formula weight FW, molecular volume V_d estimated by d and FW, molecular radius r_d estimated by V_d under the assumption of a spherical molecule ($r_d = (3V_d/4\pi)^{1/3}$), van der Waals volume V_{VDW} that is estimated by van der Waals increments,[112,113] μ, α_0, α_{anis}, and I, which are calculated using eqs 1 and 2 and quantum chemistry calculation results, for the forty molecules are also listed in Table 1. The values of μ and α_0 are also compared to the experimental data in the CRC Handbook.[108] The estimated values for more than half the molecules studied here can be compared to the experimental data in the CRC Handbook. Overall, the calculated α_0 values are quite similar to the reported data within about ±5%, except for 1,4-dioxane (about 16% smaller) and hexafluorobenzene (about 13% larger). Although the agreement for μ between the calculated and experimental data are not as good as that for α_0, the calculated μ are moderately close to the experimentally reported data (about ±10% in most cases). But some molecules with a small μ have relatively large differences (calculated μ(ethylbenzene) = 0.409 D and μ(cumene) = 0.400 D and reported μ(ethylbenzene) = 0.59 D and μ(cumene) = 0.79 D). Note that the ratios are large, but the differences are not large because of the small values themselves. These estimated molecular properties based on the quantum chemistry calculation results are important factors for intermolecular interactions. We will see the intermolecular interactions estimated from these molecular properties together with the intermolecular vibrational spectra.

In this section we briefly discuss the molecular volumes (V_d and V_{VDW}) and α_0 for the forty molecules studied here. Since OHD-RIKES detects the polarizability anisotropy relaxation and free volume is an important factors in molecular liquid dynamics, the comparisons between V_d, V_{VDW}, and α_0 could suggest whether the molecular liquids studied here are suitable for general discussion of molecular liquid dynamics or not. Figure 5a displays the relationship between V_d and V_{VDW}. Because V_d contains the free volume in liquids, V_d is larger than V_{VDW} (packing fraction $V_{VDW}/V_d = 0.56$). As shown in Figure 5a, there is a direct proportional relationship between V_d and V_{VDW}. This fact indicates that the ratios between van der Waals volumes and free volumes are not different between non-aromatic and aromatic molecular liquids measured in this study. Furthermore, there is no special molecular liquid that has a specific intermolecular interaction or packing/stacking in the present molecular liquid samples. Although aromatic molecules often show π–π interaction stacking, it does not greatly affect the density and free volume in the aromatic molecular liquids studied here.

Polarizability α is defined as the proportionality constant for the relationship between the induced dipole moment $\boldsymbol{\mu}_{ind}$ and electric field $\boldsymbol{E}$:[114]

$$\boldsymbol{\mu}_{ind} = \alpha \boldsymbol{E} \tag{8}$$

When α is divided by $4\pi\varepsilon_0$, where ε_0 is the permittivity of vacuum, α is referred as the polarizability volume. In the charge response kernel model analysis that can estimate a polarizability volume by the response of partial charge of a molecule due to the change of local electric field, it is confirmed that the polarizability volume becomes larger with a bigger volume of molecule. This is because the magnitude of delocalized charge caused by a local electric field is larger as the increase of molecular volume.[115,116] From the nature of a polarizability volume therefore, it can be expected that there is a correlation between α_0 and molecular volume V. Also, the nature of α_0 for aromatic molecules may be different from that for non-aromatic molecules, because aromatic molecules are more polarizable than non-aromatic molecules due to π electrons. Figures 5b and 5c show the plots of α_0 vs. V_{VDW} and α_0 vs. V_d, respectively. It is clear from Figures 5b and 5c that α_0 depends linearly on V_{VDW} and V_d. If the aromatic molecules showed different polarizability than non-aromatic molecules, the relation for aromatic molecules would be different from that for non-aromatic molecules. Consequently, the present forty aprotic molecular liquids are appropriate to study and consider

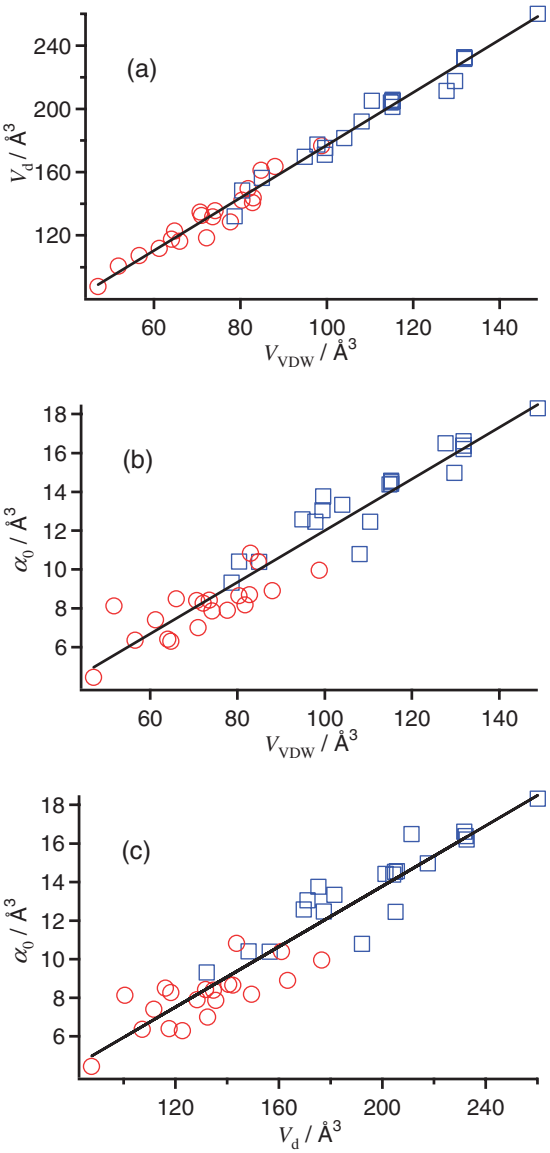

Figure 5. Plots of (a) V_d vs. V_{VDW}, (b) α_0 vs. V_{VDW}, and (c) α_0 vs. V_d. Red circles denote the values for non-aromatic molecules and blue squares denote the values for aromatic molecules. Black lines are the fits by a linear function.

the overall and general natures of intermolecular vibrational dynamics and reorientation, in a sense.

Intermolecular Vibrational Dynamics. Indeed, the detailed molecular-level understanding of intermolecular vibrations in molecular liquids is not straightforward and is difficult compared with intramolecular vibrations. There are several reasons for this difficulty of intermolecular vibrational dynamics in molecular liquids. (i) Each molecule is always fluctuating, (ii) molecular fluctuation provides different intermolecular vibrational modes, and (iii) intermolecular vibrational modes are often coupled to each other. Therefore, it is no doubt that complementary studies by spectroscopy and theory or simulation are necessary for deep and detailed understanding of intermolecular vibrational spectra in molecular liquids. Even though, overall and primary understanding of intermolecular vibrations is often useful for a global vision to the dynamics in molecular liquids. Here we attempt to obtain an overall understanding of intermolecular vibrations in molecular liquids from data of the forty aprotic molecular liquids. At first, we will discuss the shape of the intermolecular vibrational spectrum in molecular liquids. Then, we are going to compare the intermolecular vibrational spectrum with the surface tension to find a correlation between microscopic and macroscopic intermolecular interactions. The vaporization enthalpy is also used to consider the intermolecular energy in liquids. However, some liquids (e.g., polymer liquids[22] and room-temperature ionic liquids[36–38]), whose intermolecular vibrational frequency is not very different from that in normal molecular liquids, show very high boiling point at low pressure and negligible vapor pressure at ambient temperature and pressure.[117] Therefore, we choose surface tension to compare it with intermolecular vibration in this study.

Shape of Intermolecular Vibrational Spectrum: We have analyzed the broad Kerr spectra by a sum of Ohmic and anti-symmetrized Gaussian functions, as shown in Figures 4 and 6. In some recent MD simulation works for the ultrafast dynamics of molecular liquids, it is known that the molecular motions in the lower-frequency region (< ca. 50 cm^{-1}) for the intermolecular vibrational spectrum of a molecular liquid includes translational motions coupled with orientation like motions and those in the higher-frequency region (> ca. 50 cm^{-1}) are dominantly orientation like motions.[118–120] The origins of the translational and orientation like motions are mainly interaction-induced motion and libration, respectively. So, we can compare the spectral differences in low- and high-frequency regions for molecular liquids to discuss and understand a qualitative feature using the analyzed parameters.

Ricci et al. discussed the intermolecular vibrational spectrum of benzene based on a bimodal structure, which was separated into two parts, overdamped and underdamped (or Ohmic and anti-symmetrized Gaussian), along with Kubo theory.[76] Note that overdamping represents a more antisymmetric line shape and underdamping denotes a more symmetric line shape. The Kubo theory treats the two extreme cases for the spectrum line shape in dynamic systems.[121] One is a rapid fluctuation and the other one is slow. In a spectral line shape, a broad distribution of states coalesces into a narrow Lorentzian band (so-called motional narrowing) for the first case, and a broad distribution shape is represented (simple relaxation) in the latter case.

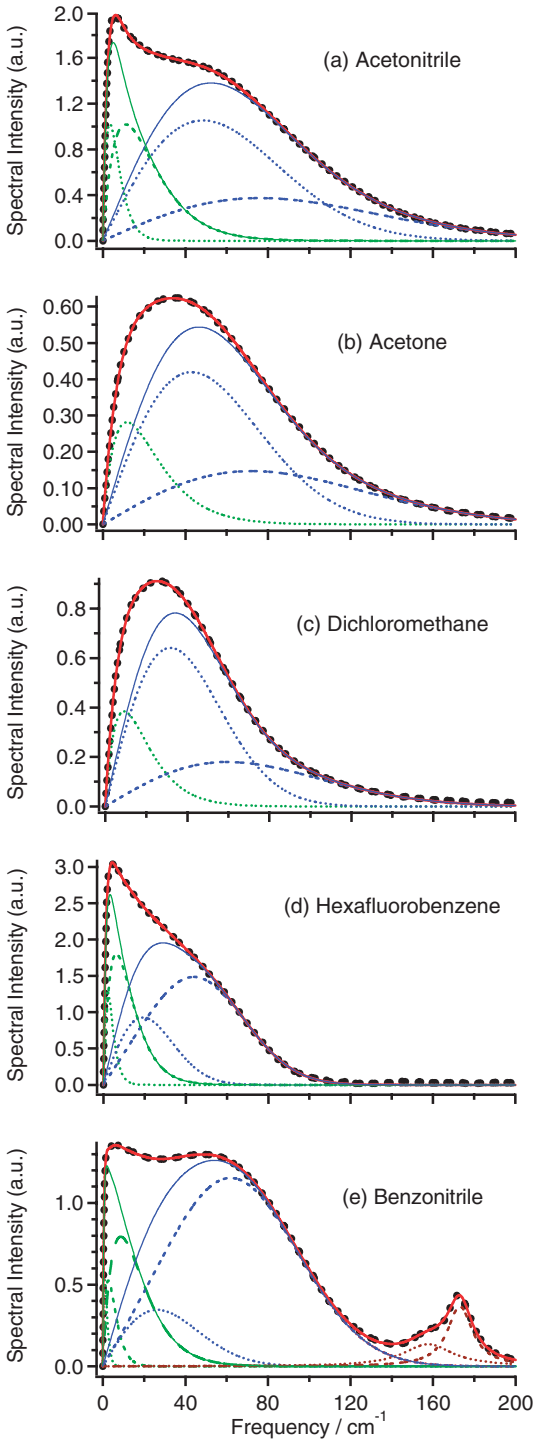

Figure 6. Fourier transform low-frequency Kerr spectra of (a) acetonitrile, (b) acetone, (c) dichloromethane, (d) hexafluorobenzene, and (e) benzonitrile. Contribution of the slowest exponential relaxation is removed in the spectra. Black dots, red lines, green lines (dotted and broken), blue lines (dotted and broken), and brown lines (dotted and broken) are data, entire fits, Ohmic functions, anti-symmetrized Gaussian functions, and Lorentzian functions (for intramolecular vibrational modes), respectively. Green and blue solid lines denote the sums of Ohmic functions and anti-symmetrized Gaussian functions, respectively.

The Kubo theory is well-used to explain the features of intramolecular cases. Ricci et al. qualitatively reproduced the temperature dependence of the intermolecular vibrational spectrum of benzene.[76] Fourkas and co-workers also explained the intermediate relaxation (low-frequency part of the broad Kerr spectrum) by Kubo theory.[71]

Besides benzene, Figure 6 displays the low-frequency Kerr spectra of acetonitrile, acetone, dichloromethane, hexafluorobenzene, and benzonitrile measured in this study as examples. The line-shape analysis results are also shown in Figure 6. As seen in Figure 6, the shape of the low-frequency Kerr spectra is really unique in each aprotic molecular liquid. For example, acetonitrile, hexafluorobenzene, and benzonitrile show a bimodal spectral shape clearly, while acetone and dichloromethane show a monotonic spectral shape. We discuss the intermolecular vibrational spectra along with treatment by Ricci et al.[76] below.

In Figure 6, there are many fitting functions to express the broad intermolecular vibrational spectrum in molecular liquids. We classify the intermolecular vibrational spectrum into two parts: overdamped and underdamped parts. A sum of Ohmic functions is categorized into an overdamped part and a sum of anti-symmetrized Gaussian functions is treated as an underdamped part. So the two distinguished parts are displayed in each low-frequency Kerr spectrum shown in Figure 6. The idea of the damping factor is of the multi-mode Brownian oscillator model,[105–107] but it is no doubt that the line shape of an Ohmic function is overdamped and that of an anti-symmetrized Gaussian function is underdamped for the line shapes. This classification to a broad spectrum may be too simple and arbitrary, while it can be worthwhile to consider the general shape of the intermolecular vibrational spectrum in molecular liquids simply.

Figure 7a shows the plots of ω_O vs. ω_G and Figure 7b shows plots of $\Delta\omega_O$ vs. $\Delta\omega_G$. ω_O, $\Delta\omega_O$, ω_G, and $\Delta\omega_G$ are the peak frequency and width (FWHM) of the bands of the sum of Ohmic functions and the sum of anti-symmetrized Gaussian functions. These parameters are summarized in Supporting Information. As displayed in Figures 7a and 7b, it seems that there is no correlation between the underdamped and overdamped motions in the band peak and width. Figure 7c shows the plots of the peak frequencies ω vs. the widths $\Delta\omega$ (ω_O vs. $\Delta\omega_O$ and ω_G vs. $\Delta\omega_G$). As clearly found in Figure 7c, there is a linear correlation between them. Actually, this is not very surprising. The low-frequency side of a low-frequency spectrum is zero, so the spectral broadening in the low-frequency part is limited to the zero frequency. As a result, a vibrational band located at a higher-frequency region has a wider spectral width than that located at lower frequency, when the two bands have an identical broad band width. Figure 7d shows the plots of the first moment of spectrum M_1 vs. $\Delta\omega_{inter}$ for the forty aprotic molecular liquids. $\Delta\omega_{inter}$ is the width (FWHM) of the low-frequency Kerr spectrum subtracted clear intramolecular vibrational modes. We can confirm a monotonic increase of the characteristic frequency with the broader spectral width in the low-frequency Kerr spectrum. This reflects the relation between ω and $\Delta\omega$ shown in Figure 7c.

In Figure 7c, we find a notable fact: the band peak (and width) of an Ohmic band is apart from that of an anti-

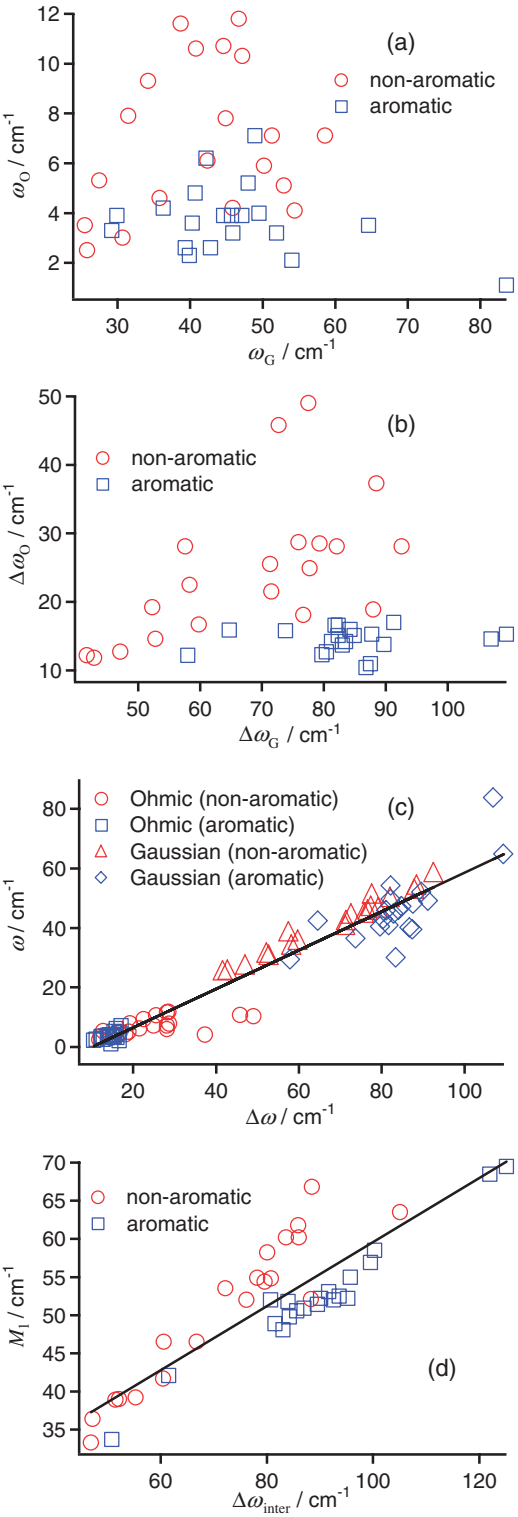

Figure 7. Plots of (a) ω_O vs. ω_G, (b) $\Delta\omega_O$ vs. $\Delta\omega_G$, (c) ω vs. $\Delta\omega$ (ω_O vs. $\Delta\omega_O$ and ω_G vs. $\Delta\omega_G$), and (d) M_1 vs. $\Delta\omega_{inter}$. Red symbols are for non-aromatic molecular liquids and blue symbols are for aromatic molecular liquids.

symmetrized Gaussian band for aromatic molecular liquids, but non-aromatic molecular liquids show one broad unimodal distribution. Namely, aromatic molecular liquids show a clear bimodal spectrum, but the monomodality or bimodality of the

spectral shape of non-aromatic molecular liquids depends on the molecular liquid. Ricci et al. simulated the temperature dependence of the shape of the intermolecular vibrational band for benzene based on Kubo theory, as mentioned before.[76] They showed that a bimodal spectral shape appeared in the case of the normal relaxation limit and a monotonic spectrum (motional narrowing) was reproduced in the case of the fast modulation limit. Fourkas and co-workers observed that the intermolecular vibrational spectra of acetonitrile and carbon disulfide showed more bimodal character with decreased temperature.[70] In the molecular liquids studied here, several non-aromatic molecular liquids such as dichloromethane, carbon disulfide, and carbon tetrachloride, which show small differences between ω_O and ω_G, may be in a fast fluctuation limit to show a motional narrowing, but aromatic molecular liquids are likely to fluctuate more slowly than the motional narrowing limit.

On the other hand, Zhong and Fourkas showed that the low-frequency Kerr spectral shape in some aromatic molecular liquids like benzene was rectangular and that in some other aromatic molecular liquids like hexafluorobenzene was triangular.[74] They explained the shape of the low-frequency Kerr spectrum in molecular liquids for the molecular shape in accordance with the MD simulation and instantaneous normal mode analysis results by Stratt and co-workers.[119,122] Their simulation results well reproduced the spectral similarity between the Kerr spectra of benzene and biphenyl, which was experimentally observed by Quitevis and co-workers.[99] In the simulation of benzene, Ryu and Stratt found that the first shell molecules contributed dominantly to the Kerr spectrum and pointed out that the dynamics in polarizability was mostly driven by single-molecule motion.[119] Conversely, Elola and Ladanyi pointed out from their MD simulation results that the shapes of Kerr spectra of benzene, trifluorobenzene, and hexafluorobenzene were largely determined by the strengths of the pairwise potentials in the three liquids.[123] Because the spectral shapes in the liquids did not well correlate to their dipole moments, Zhong and Fourkas concluded that the molecular shape played a major role in determining the Kerr spectral shape.[74]

If we look at Figure 7c based on the idea of the molecular shape,[74,119,122] the general spectral difference between aromatic and non-aromatic molecular liquids can be due to the phenyl ring. This is probably because aromatic molecules have their unique bulky flat ring and unique librational motion for the phenyl ring.[119,122] Therefore, the shape of Kerr spectra is possibly driven largely by the molecular shape for aromatic molecular liquids. This begs the question of how the spectra of aliphatic systems differ from those of aromatic systems. If the molecular shape (or rotational time constant) plays a great role in the intermolecular vibrational spectrum, we would observe a correlation between ω_G/ω_O and a molecular shape factor. ω_G/ω_O means that the larger value denotes more bimodal character and the smaller value denotes more monomodal character. Figure 8 plots of (a) ω_G/ω_O vs. α_{anis} and (b) ω_G/ω_O vs. B_x/B_z. B_x and B_z, which have been estimated by ab initio quantum chemistry calculation, are the rotational constants for the fast axis and slow axis, respectively. The reason for these plots is finding a correlation between the bimodality of spectra and

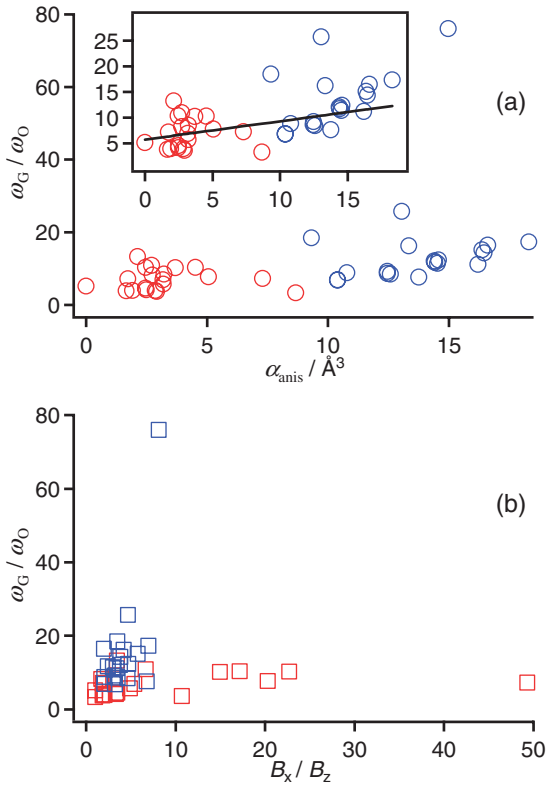

Figure 8. Plots of ω_G/ω_O vs. (a) α_{anis} and (b) B_x/B_z. Red symbols denote non-aromatic molecular liquids and blue symbols denote aromatic molecular liquids. Inset expands the scale.

molecular shape (or molecular anisotropy). As shown in Figure 8, both α_{anis} and B_x/B_z have almost no correlation to ω_G/ω_O, while ω_G/ω_O and α_{anis} show a very weak correlation except for the value for 1-butylimidazole (Figure 8a inset). Therefore, it is hard to give a clear answer for the relationship between molecular shape and spectral bimodality, but it may be plausible that phenyl rings contribute uniquely to the intermolecular vibrational spectrum as shown in Figure 7c.

Regarding the intermolecular interaction in molecular liquids, we still think that the intermolecular interaction also has an important role in the intermolecular vibrational spectrum in molecular liquids. Meech and co-workers indicated from their experimental study of liquid sulfur oxide and its mixtures that the temperature dependence of a center frequency for the intermolecular vibrational band (librational components) was attributed to intermolecular interactions.[124] We will show evidence for a relationship between the Kerr spectrum and intermolecular force in molecular liquids in the successive subsection (Note that the Kerr spectrum here means a characteristic frequency, the first moment of a spectrum, not spectral shape, vide infra). In any case, it has become clear from this study that the intermolecular vibrational spectrum in aromatic molecular liquids is clearly bimodal, but in non-aromatic molecular liquids it depends on the liquid.

Comparison with Surface Tension: Intermolecular vibrational spectra in molecular liquids include information on the molecular level. As mentioned above, however, under-

standing the spectral characteristics of intermolecular vibration in molecular liquids is not simple, straightforward, or easy. On the other hand, it is very useful to understand the relation between intermolecular vibration and a bulk properties for molecular liquids if it exists. In this section, we compare intermolecular vibrational spectra with the surface tension to find a correlation between microscopic and macroscopic properties related to the intermolecular interaction in molecular liquids. For this purpose, we consider the first moment of spectrum M_1 in the broad intermolecular vibrational spectrum here. This aspect of intermolecular vibration based on a single characteristic frequency of the broad spectrum (e.g., peak and M_1) may be too simple and crude, while we can think generally of the intermolecular vibrational spectrum in molecular liquids using a single value.

At the starting point, let us consider the vibration of a diatomic molecule as a (one-dimensional) harmonic oscillator. This treatment neglects the multi-dimensionality and anharmonicity of the vibrational mode, but it is helpful in understanding it by contemplating a simple model. The characteristic frequency $\tilde{\nu}$ in wavenumbers of a harmonic oscillator is given by,

$$\tilde{\nu} = \frac{1}{2\pi c}\sqrt{\frac{k}{m_R}} \tag{9}$$

where c is the velocity of light, k is the force constant, and m_R is the reduced mass. Although the intermolecular vibration is, of course, different from the intramolecular vibration, the scheme of a harmonic oscillator is suggestive for an overall understanding of intermolecular vibration. According to eq 9, an intermolecular vibration is related to the reduced mass and intermolecular interaction.

One can think that surface tension is a macroscopic physical property of the intermolecular force. Figure 9a is the plots of M_1 for intermolecular vibrational spectrum vs. $(\gamma/\mathrm{FW})^{1/2}$. The idea of the plots is finding whether a correlation between the microscopic intermolecular interaction (M_1) and bulk property (γ) is there or not, along with the scheme of a harmonic oscillator (eq 9). As seen in Figure 9a, we have found that the correlations between M_1 and $(\gamma/\mathrm{FW})^{1/2}$ for non-aromatic liquids and aromatic liquids are totally different and the correlations between M_1 and $(\gamma/\mathrm{FW})^{1/2}$ for both the non-aromatic and aromatic molecular liquids are weak, particularly for non-aromatic molecular liquids (linear correlation coefficient $R = 0.7356$ for non-aromatic molecular liquids and $R = 0.7968$ for aromatic molecular liquids). In contrast to Figure 9a, there is a moderate correlation between M_1 and $(\gamma/d)^{1/2}$ for all forty molecular liquids ($R = 0.8426$), as shown in Figure 9b that plots M_1 vs. $(\gamma/d)^{1/2}$. Although the correlation between M_1 vs. $(\gamma/d)^{1/2}$ for aromatic molecular liquids ($R = 0.7902$) is similar to the correlation between M_1 and $(\gamma/\mathrm{FW})^{1/2}$, the correlation between M_1 vs. $(\gamma/d)^{1/2}$ for non-aromatic molecular liquids ($R = 0.9041$) is substantially good compared to the correlation between M_1 and $(\gamma/\mathrm{FW})^{1/2}$ and that shows for all forty molecular liquids. The difference between γ/FW and γ/d is the unit of space. γ/FW is for a molecule (or molecules), and γ/d is for volume. What does the fact imply? Also, why does the surface tension have a correlation to the frequency of vibration?

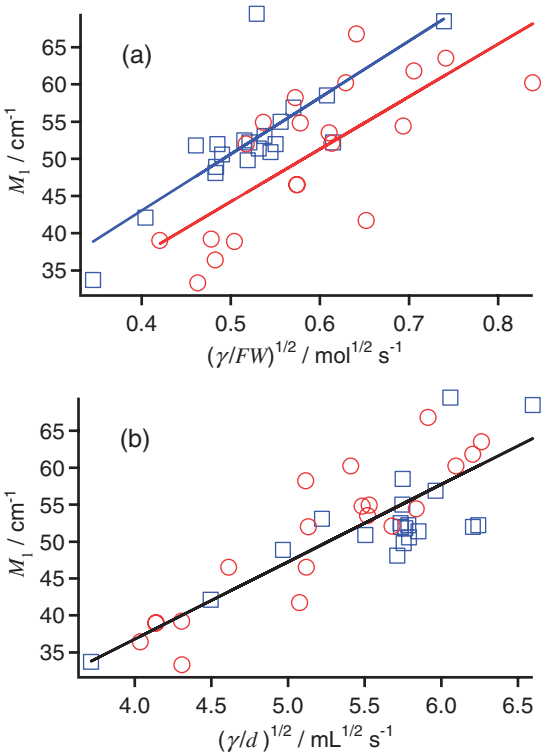

Figure 9. Correlations between (a) M_1 and $(\gamma/\mathrm{FW})^{1/2}$ and (b) M_1 and $(\gamma/d)^{1/2}$. Red circles denote the values for non-aromatic molecules and blue squares denote the values for aromatic molecules. Red, blue, and black lines are linear function fits for aromatic, non-aromatic, and all molecular liquids, respectively.

It may be worth considering a correlation between the simple intermolecular interaction energy of two identical molecules and the intermolecular vibration (M_1) at the beginning. The intermolecular interaction energy of two identical neutral molecules in the Lennard–Jones potential expression is written by,[114,125]

$$U(r) = \frac{C_{rep}}{r^{12}} - \frac{1}{r^6}(C_{d\text{–}d} + C_{d\text{–}id} + C_{disp}) \tag{10}$$

where r is the distance between molecules, C_{rep}, $C_{d\text{–}d}$, $C_{d\text{–}id}$, and C_{disp} are the coefficients for the repulsion, dipole–dipole interaction, dipole–induced dipole interaction, and dispersion interaction, respectively. The coefficients for the attractive term are given by,[114,125]

$$C_{d\text{–}d} = \frac{2\mu^4}{3(4\pi\varepsilon_0)^2 k_B T} \tag{11}$$

$$C_{d\text{–}id} = \frac{2\alpha_0\mu^2}{(4\pi\varepsilon_0)^2} \tag{12}$$

$$C_{disp} = \frac{3}{4}\frac{I{\alpha_0}^2}{(4\pi\varepsilon_0)^2} \tag{13}$$

where ε_0 is the permittivity of a vacuum. Here, we discuss the intermolecular interaction energy U_{r0} that is the value at the equilibrium distance between the two molecules ($r_0 = 2r_d$). Because C_{rep} is often treated as an adjustable parameter,[114,126] we have estimated U_{r0} as follows. At the equilibrium distance r_0, the derivative of $U(r)$ by r is 0. Accordingly, we can

calculate U_{r0} as,

$$U_{r0} = -\frac{1}{2r_0{}^6}(C_{d\text{–}d} + C_{d\text{–}id} + C_{disp}) \quad (14)$$

Values of $C_{d\text{–}d}/r_0{}^6$, $C_{d\text{–}id}/r_0{}^6$, $C_{disp}/r_0{}^6$ and U_{r0} for all forty molecules are summarized in Supporting Information.

Figure 10a shows the plots of M_1 vs. $-U_{r0}$ for the forty aprotic molecular liquids studied here. In distinction from the plots of M_1 vs. $(\gamma/d)^{1/2}$ (Figure 9b), the correlation between M_1 and U_{r0} is not good, as clearly found in Figure 10a. There are two plausible reasons for the poor correlation between M_1 and $-U_{r0}$. First, the physical properties, μ, α_0, and I, are calculated in the gas phase. Second, U_{r0} calculated here is of the pure intermolecular interaction between two identical molecules (no contribution from many-body interaction).

Figure 10b shows the plots of M_1 vs. $-U_{r0}$ for eight molecular liquids (vide supra) including the dielectric medium effect. For U_{r0} in these plots, the physical properties, μ, α_0, and I, include the dielectric medium effect (IEF-PCM) as well. Also, the dielectric constants of solvents (ε_s) are included in eqs 11–13 to calculate U_{r0} (ε_0 is replaced by $\varepsilon_0\varepsilon_s$). A clear correlation between M_1 vs. $-U_{r0}$ does not exist in aprotic molecular liquids shown in Figure 10b. Although Figure 10b suggests that aromatic molecules may show a linear correlation between M_1 vs. $-U_{r0}$, some aromatic molecules showing small M_1 values in intermolecular vibrational spectra do not fit the correlation well. Therefore, the bimolecular interaction is most likely minor for the intermolecular vibration in aprotic molecular liquids.

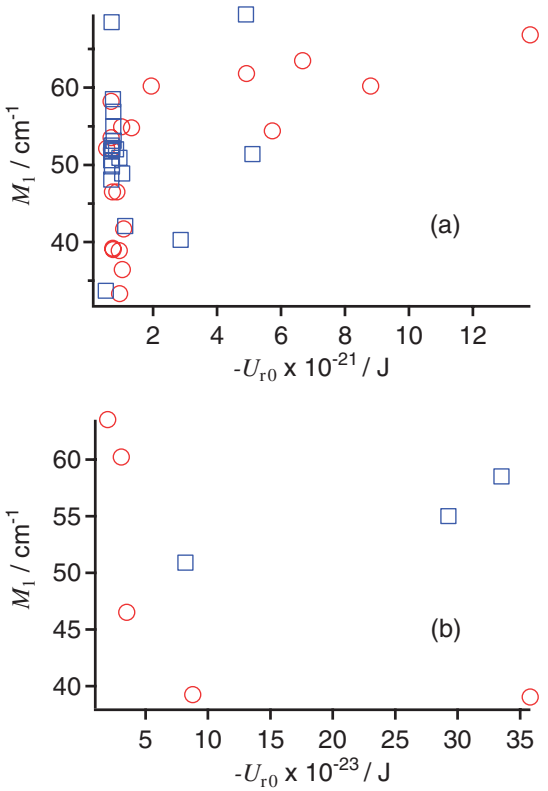

Figure 10. Plots of M_1 vs. $-U_{r0}$ for (a) gas-phase and (b) dielectric medium. Red circles denote the values for non-aromatic molecules and blue squares denote the values for aromatic molecules.

As we showed in Figures 9 and 10, the bimolecular interaction energy is not related to the spectral frequency, but the square root of the value of surface tension divided by density (and also $(\gamma/\mathrm{FW})^{1/2}$ for aromatic molecular liquids) has a correlation with M_1. Surface tension is a property of intermolecular force in liquid. The force is for liquid surfaces, but the intermolecular force for molecules works in three dimensions in liquid at a microscopic level. Also, molecules in liquids always interact with several neighboring molecules and never interact with only a single molecule. As well as intermolecular interaction, intermolecular vibrational motions for molecules in liquids are influenced by the neighboring molecules. Therefore, the present results indicate that the many-body interaction effect may be important for the (collective) intermolecular interaction in molecular liquids, and thus the characteristic frequency M_1 of the intermolecular vibrational band seems to be correlated to intermolecular interaction. Furthermore, the correlation between M_1 and $(\gamma/d)^{1/2}$ is better than that between M_1 and $(\gamma/\mathrm{FW})^{1/2}$. If we take molecular weight and density into consideration for the two relationships, mass per volume (density) accounts for three dimensionality and many-body interaction in molecular liquids, while a simple single mass itself (reduced mass) is just for a simple vibrational oscillator.

We might add a comment on the relationship between the Hildebrand solubility parameter, which is related to the cohesive energy, and surface tension. Recently, Jin et al. showed linear relationships between the square root of the Hildebrand solubility parameter and the surface tension divided by the cubic of molar volume that was estimated from d and FW in a series of molecular liquids.[127] Although the relation depends on the series of molecular liquids, it is linear within a category of solvents, such as aprotic solvents, hydrogen-bonding liquids, or alkali halides. These results suggests that a parameter of the surface tension and molar volume correlates with the intermolecular interaction in bulk (not bimolecular interaction).

Besides the intermolecular interaction, we should consider the other possibilities for the correlation and intermolecular vibrational spectrum. It is no doubt that the effect of anharmonicity of the intermolecular vibrational modes is there in the intermolecular vibrational spectrum for molecular liquids. However, we do not know the magnitude of the anharmonicitiy of the intermolecular vibrational modes in each molecular liquid. Also, we do not know if they are almost the same for all the sample molecular liquids studied here. Furthermore, we have no idea how many distinguished intermolecular vibrational modes exist in the broad spectrum of each molecular liquid. MD simulation is promising to provide these aspects. However, at least we expect that the correlation between M_1 vs. $(\gamma/d)^{1/2}$, which comes from a symmetric vibrational oscillator, should not exist if anharmonicitiy is very important and that is dependent on the molecular liquid.

In contrast to the harmonic oscillator, librational motion that locates at the higher-frequency region in the broad intermolecular vibrational spectrum is similar to rotation. Therefore, it may be worthwhile to compare ω_G with rotational constants. Figure 11 shows the plots of ω_G vs. (a) B_x (fast rotational constant), (b) B_z (slow rotational constant), and (c) B_{av} (average

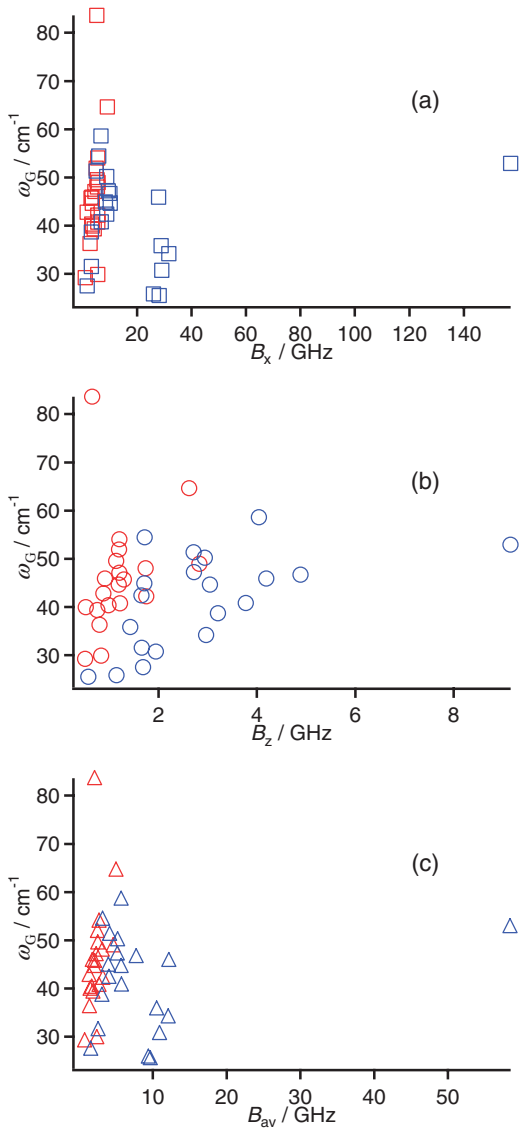

Figure 11. Plots of ω_G vs. (a) B_x, (b) B_z, and (c) B_{av}. Red symbols denote non-aromatic molecular liquids and blue symbols denote aromatic molecular liquids.

of the three rotational constants). The rotational constants are obtained by the stabilized structures of molecules obtained by ab initio quantum chemistry calculation based on the B3LYP/aug-cc-pVDZ level of theory. As clearly shown in Figure 11, there are no clear correlations between ω_G and rotational constants. This indicates that the librational motion is not simply governed by the single molecular rotation, which implies the importance of the intermolecular interaction.

We still do not address why aromatic molecular liquids show a linear relation between M_1 vs. $(\gamma/\mathrm{FW})^{1/2}$ except for 1-butylimidazole ($M_1 = 69.5\,\mathrm{cm}^{-1}$ and $(\gamma/\mathrm{FW})^{1/2} = 0.529\,\mathrm{mol}^{1/2}\,\mathrm{s}^{-1}$), as well as M_1 vs. $(\gamma/d)^{1/2}$ (Figure 9). Because the surface tension is a parameter for both relations, the intermolecular interaction for many molecules influences intermolecular vibration. FW is the weight of a molecule, but d is a weight per volume that includes free volume. If we compare FW and d between non-aromatic molecular liquids and aromatic molecular liquids, the ranges of FW and d for aromatic molecular liquids are smaller than those for non-aromatic molecular liquids. This difference might provide a better correlation of M_1 and $(\gamma/d)^{1/2}$ than M_1 and $(\gamma/\mathrm{FW})^{1/2}$ for non-aromatic molecular liquids and similar quality correlations of M_1 and $(\gamma/d)^{1/2}$ and M_1 and $(\gamma/\mathrm{FW})^{1/2}$ for aromatic molecular liquids. Also, we should also be reminded that π–π interaction for aromatic molecules occurs in the (one-dimensional) out-of-plane direction for the phenyl ring. This effect of the intermolecular interaction arising from the unique molecular shape may give a moderate correlation between M_1 and $(\gamma/\mathrm{FW})^{1/2}$.

As discussed before, Zhong and Fourkas have pointed out the importance of molecular shape on the spectrum shape.[74] From our previous study of the comparison between an ionic liquid (*N*-(2-methoxyethyl)pyridinium dicyanoamide) and a neutral binary mixture of a pair of isoelectronic and homomorphous molecules of the ionic liquid constituents (methoxyethylbenzene and dicyanomethane), it has been clear that the spectral shapes of the ionic liquid and neutral binary solution are similar, while the spectrum for the ionic liquid locates at higher frequency than that for the neutral binary mixture.[128] Because the intermolecular interaction for ionic liquids is stronger than that for neutral molecular liquids, the difference in the characteristic frequency for the intermolecular vibrational band in molecular liquids mainly comes from the difference in the intermolecular interaction. This result also points out that the characteristic frequency depends on the intermolecular interaction and similar molecular shape gives similar spectral shape. Therefore, we conclude that the characteristic frequency such as M_1 is related to the intermolecular interaction and the molecular shape, particularly phenyl rings (and also motional narrowing arising from the molecular shape), likely contributes to the spectral shape largely.

At the end of this subsection, we would also like to state that finding the correlation between the microscopic intermolecular vibration and macroscopic surface tension in molecular liquids is the first report and the major result in this study.

Reorientation. Overdamped decays of the Kerr transients for the forty molecular liquids have been analyzed by a multiexponential function. The fit parameters for the molecular liquids are summarized in Table 2. Figures of the Kerr transients and the fits for all forty molecular liquids measured in this study are summarized in Supporting Information. Note that carbon tetrachloride does not show overdamped decay in the Kerr transient because of the spherical symmetry.

Reorientation of a single molecule in solution is well discussed based on the Stokes–Einstein–Debye (SED) hydrodynamic model.[129–131] The reorientation time of a single molecule τ_{rs} in the SED model is expressed by

$$\tau_{rs} = \frac{V\eta f C}{k_B T} + \tau_{rs0} \tag{15}$$

where V is the solute volume, η is the shear viscosity of medium, k_B is the Boltzmann constant, T is the absolute temperature, f is the solute shape factor, C is the solute–medium coupling factor that is determined by the hydrodynamic boundary conditions, and τ_{rs0} is the intrinsic reorientation time (free-rotator correlation time at zero viscosity). In the simplest SED model, f and C are unity and τ_{rs0} is zero. Equation 15 therefore can be rewritten as,

$$\tau_{rs} = \frac{V\eta}{k_B T} \tag{16}$$

This equation has been used for not only a solute in solution, but also neat liquids. Actually, RIKES observes a collective reorientation correlation time in liquids, not a single molecule reorientation.[71] Equation 17 gives the relationship between the characteristic time constants of the collective and single molecular reorientations.

$$\tau_{rc} = \frac{g_2}{j_2}\tau_{rs} \tag{17}$$

where g_2 is the static orientation pair correlation parameter and j_2 is the dynamic orientation pair correlation parameter.[129] The ratio g_2/j_2 is still an open question and most of the values for the forty molecular liquids measured here are not available. Therefore, we simply think of a reorientation time in terms of the single molecule reorientation scheme (eq 17). The primary purpose in this study is a whole and simple understanding of the nature of diffusive relaxation in neat aprotic molecular liquids.

The relaxation time constants in the long time Kerr transients for the molecular liquids have been estimated from the fit (from 3 ps) by a multi-exponential function. A non-exponential behavior in picosecond Kerr transients for molecular liquids is well-recognized even in symmetric top molecules.[50,71,73] There is some argument over the origin of the intermediate relaxation. Fourkas and co-workers proposed that the faster quasi-exponential relaxation arises from a spectral diffusion (motional narrowing).[71] McMorrow et al. analyzed the sub-picosecond Kerr transient of CS_2 in a unified manner in terms of an inhomogeneously broadened harmonic oscillator model for a single intermolecular vibrational coordinate.[50] This model shows bimodal character: a Gaussian-like ultrafast relaxation and a slower exponential-like relaxation. The exponential-like relaxation depends on the relationship between the vibrational oscillator frequency and dephasing frequency. In either way, this process represents the crossover between the underdamped intermolecular vibrations and slowest diffusive relaxation (α relaxation).

At first, Figure 12 shows (a) τ_{slow} vs. ηV_d and (b) τ_{slow} vs. ηV_{VDW} for the molecular liquids studied here. The difference between Figures 12a and 12b is the absence/presence for the effect of free volume. As displayed in Figure 12, both cases show a modestly good linear relationship between the relaxation time and the product of shear viscosity and molecular volume. Namely, the slowest relaxation time observed in Kerr transients is correlated to ηV for the molecular liquids overall. Both the relationships are not very different, but τ_{slow} vs. ηV_d (Figure 12a, $R = 0.9464$) is slightly better than τ_{slow} vs. ηV_{VDW} (Figure 12b, $R = 0.9438$). It is well-known that the collective reorientation time for molecular liquids observed by RIKES obeys the SED hydrodynamic model.[19,71,73] As also shown in Figure 12, the extrapolated τ_{slow} value to $V_d\eta$ or $V_{VDW}\eta = 0$ is close to 0. Namely τ_{rs0} is nearly zero. Temperature-dependence studies showed that τ_{rs0} depended on the target molecule and it was unnecessary to be 0.[58,71,74–76,124,132] The slope is 0.0646 (ps cP^{-1} Å^{-3}). Since the slope should be 0.244 (ps cP^{-1} Å^{-3}) in the case of eq 16 (single molecular

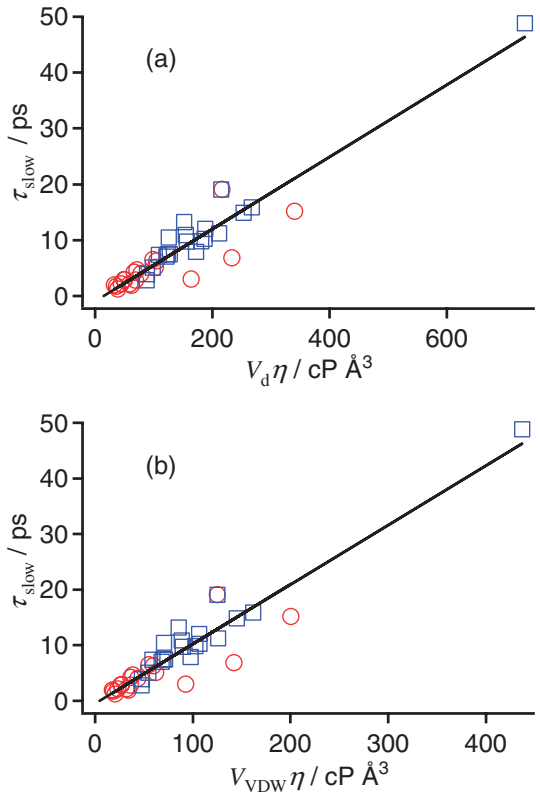

Figure 12. Comparison between plots of (a) τ_{slow} vs. $V_d\eta$ and (b) τ_{slow} vs. $V_{VDW}\eta$. Red circles show the values for non-aromatic molecules and blue squares show the values for aromatic molecules. Liner function fits are also shown by black lines.

reorientation), the actual relaxation time is faster than the time predicted by eq 16. Therefore, C in eq 15 for the reorientation in neat liquids is for the slip condition. Also, the disagreement between the observed and predicted characteristics may be the different relaxation times (the observed τ_{slow} is for the collective reorientation and τ_{rs} in eq 16 is for the single molecular reorientation). Similar observations have been reported for liquids and solutions.[133–135] Because the shape factor f in eq 15 depends on molecule, the discussion on the molecular shape based on the SED model might be exceed. However, aromatic molecular liquids show a better correlation than non-aromatic molecular liquids, if we carefully look at Figure 12. This fact might imply that the phenyl ring gives a similar f value for the present aromatic molecules and has an important role on the reorientation in aromatic molecular liquids.

SED plots for five different molecular liquids were recently shown by Zhong and Fourkas.[74] They are dependent on molecular liquids. Furthermore, the ratio g_2/j_2 also depends on molecular liquids, as mentioned above. So, a single relation between the relaxation time and the product of volume and shear viscosity for all the forty molecular liquids studied here is unnecessary. Nonetheless, the SED plots for the molecular liquids shown in Figure 12 may imply that the reorientation in molecular liquids is rather general and the major factors for reorientation in neat aprotic liquids are shear viscosity, mo-

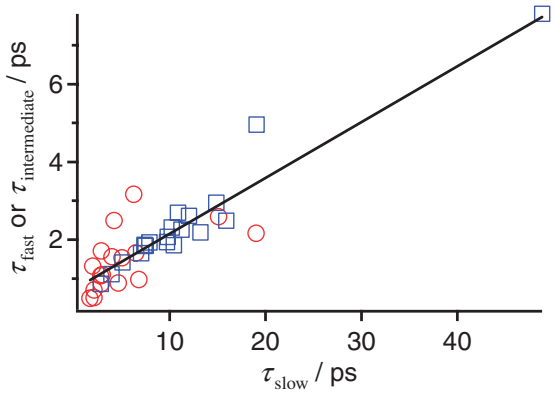

Figure 13. Plots of τ_{fast} or $\tau_{intermediate}$ vs. τ_{slow}. Red circles indicate the values for non-aromatic molecules and blue squares indicate the values for aromatic molecules. Fit by a linear function is also shown.

lecular volume, and temperature rather than the molecular shape and static and dynamic orientation pair correlation parameters.

As briefly mentioned previously, a non-exponential behavior for picosecond Kerr transients is observed even in symmetric top molecules.[50,71,73] Fourkas and co-workers indicated that an intermediate relaxation, which was in between the slowest relaxation and intermolecular vibrational dynamics, in some pure molecular liquids showed the SED hydrodynamic behavior in the same way as the slowest relaxation time.[71,73] Figure 13 shows the plots of τ_{slow} vs. $\tau_{intermediate}$ or τ_{fast}. τ_{slow} is the slowest relaxation time as mentioned before. $\tau_{intermediate}$ is τ_2 for sample liquids showing tri-exponential relaxation behavior, and τ_{fast} is τ_1 for molecular liquids showing bi-exponential relaxation. As seen in Figure 13, there is a moderate linear correlation between τ_{slow} vs. $\tau_{intermediate}$ or τ_{fast}. This was also observed in some simple molecular liquids by Fourkas and co-workers.[71,73] This fact suggests that the slower structural relaxation is governed by the intermediate relaxation process. We also note that the relationship between the slowest and intermediate relaxation processes is however different from the relation between the underdamped and overdamped motions in intermolecular vibrations described before (Figure 7a).

Summary

In this study, we investigated ultrafast dynamics in aprotic molecular liquids at ambient temperature. Data of twenty non-aromatic and twenty aromatic molecular liquids were collected for primary understanding of ultrafast molecular dynamics (intermolecular vibrational dynamics and collective reorientation). For this purpose, shear viscosities, densities, and surface tensions of the forty aprotic molecular liquids were also measured in this study. Ab initio quantum chemistry calculations based on the level of theory of B3LYP/aug-cc-pVDZ were also made to calculate the molecular properties, e.g., dipole moment, polarizability volume, and ionization energy, which were used for the estimations of the pure intermolecular interaction energies of two identical molecules.

From the results of the Fourier transform Kerr spectra, we discussed the nature of spectral shape of intermolecular vibration in the liquids. We found that aromatic molecular liquids showed clear bimodal spectral characteristics, but the spectra for non-aromatic molecular liquids was dependent on the liquid: some of them were clearly bimodal and some were monomodal. There are two possibilities for the bimodal aromatic molecular liquids. One is molecular shape and another one is motional narrowing of intermolecular vibration. Because the studied aromatic molecular liquids have large and flat ring structures, the intermolecular vibrational dynamics in aromatic molecular liquids is different from that in non-aromatic molecular liquids. From the view point of Kubo theory, aromatic molecular liquids are not in the clear motional narrowing condition, while the non-aromatic molecular liquids depend on molecule. The two different conditions between aromatic and non-aromatic molecular liquids may arise from the different molecular shapes: aromatics have a phenyl ring, but non-aromatics do not.

In a comparison of the intermolecular vibrational spectrum with surface tension, we also found that the first moment of broad low-frequency Kerr spectra correlated to the square root of the value of surface tension divided by density. This result indicates that the microscopic intermolecular interaction (intermolecular vibrational spectrum) is related to the macroscopic properties of the molecular liquid. However, we cannot confirm a clear correlation between the first moment of low-frequency Kerr spectra and the pure intermolecular interaction energy of two identical molecules. This fact indicates that many-body interaction likely influences the intermolecular vibration in molecular liquids, and pure bimolecular interaction is insufficient to represent the nature of the intermolecular vibration in molecular liquids.

In the slow diffusive reorientation for molecular liquids, we reconfirmed that the picosecond diffusive relaxation in Kerr transients of molecular liquids showed a non-exponential behavior. The slowest relaxation is due to collective reorientation, and the relaxation time is qualitatively explained by the simple Stokes–Einstein–Debye hydrodynamic model. The characteristic time of the intermediate relaxation between the intermolecular vibrational dynamics and slowest diffusive relaxation also has a moderate linear correlation with the slowest relaxation time. Namely, the intermediate relaxation governs the slowest diffusive relaxation. This is different from the relationship between the overdamped and underdamped motion in intermolecular vibrational dynamics.

We thank Dr. Yuki Nagata (BASF SE), Prof. Tateki Ishida (Institute for Molecular Science), Prof. Edward W. Castner, Jr. (Rutgers University), Prof. Mark Maroncelli (Pennsylvania State University), and Prof. Stephen R. Meech (University of East Anglia) for helpful discussions and/or critical readings of this manuscript. This study was partially supported by the Ministry of Education, Culture, Sports, Science and Technology (MEXT) of Japan (Grant-in-Aids for Scientific Research (C): No. 19559001 and Young Scientists (A): No. 21685001 (HS) and Grant-in-Aid for Priority Area "Science of Ionic Liquids:" No. 17073002 (KN)). This work was also supported in part by the JGC-S Scholarship Foundation and the Izumi Science and Technology Foundation (HS).

Supporting Information

Kerr transients and their fits and Fourier transform Kerr spectra and their fits for all forty molecular liquids measured in this study are summarized. Quantum chemistry calculation results including the solvent dielectric effect (IEF-PCM) are also summarized, as well as molecular properties based on the quantum chemistry calculation result including dielectric medium effect and parameters for intermolecular interaction energies. This material is available free of charge on the web at http://www.csj.jp/journals/bcsj/.

References

1 P. F. Barbara, W. Jarzeba, *Adv. Photochem.* **1991**, *15*, 1.
2 M. Maroncelli, *J. Mol. Liq.* **1993**, *57*, 1.
3 H. Heitele, *Angew. Chem., Int. Ed. Engl.* **1993**, *32*, 359.
4 K. Yoshihara, K. Tominaga, Y. Nagasawa, *Bull. Chem. Soc. Jpn.* **1995**, *68*, 696.
5 G. R. Fleming, M. Cho, *Annu. Rev. Phys. Chem.* **1996**, *47*, 109.
6 W. P. de Boeij, M. S. Pshenichnikov, D. A. Wiersma, *Annu. Rev. Phys. Chem.* **1998**, *49*, 99.
7 N. Nandi, K. Bhattacharyya, B. Bagchi, *Chem. Rev.* **2000**, *100*, 2013.
8 S. K. Pal, A. H. Zewail, *Chem. Rev.* **2004**, *104*, 2099.
9 K. Ohta, K. Tominaga, *Bull. Chem. Soc. Jpn.* **2005**, *78*, 1581.
10 M. L. Horng, J. A. Gardecki, A. Papazyan, M. Maroncelli, *J. Phys. Chem.* **1995**, *99*, 17311.
11 L. Reynolds, J. A. Gardecki, S. J. V. Frankland, M. L. Horng, M. Maroncelli, *J. Phys. Chem.* **1996**, *100*, 10337.
12 P. Vöhringer, N. F. Scherer, *J. Phys. Chem.* **1995**, *99*, 2684.
13 F. O. Raineri, H. L. Friedman, *Adv. Chem. Phys.* **1999**, *107*, 81.
14 D. McMorrow, W. T. Lotshaw, G. A. Kenney-Wallace, *IEEE J. Quantum Electron.* **1988**, *24*, 443.
15 W. T. Lotshaw, D. McMorrow, N. Thantu, J. S. Melinger, R. Kitchenham, *J. Raman Spectrosc.* **1995**, *26*, 571.
16 S. Kinoshita, Y. Kai, T. Ariyoshi, Y. Shimada, *Int. J. Mod. Phys. B* **1996**, *10*, 1229.
17 E. W. Castner, Jr., M. Maroncelli, *J. Mol. Liq.* **1998**, *77*, 1.
18 N. A. Smith, S. R. Meech, *Int. Rev. Phys. Chem.* **2002**, *21*, 75.
19 Q. Zhong, J. T. Fourkas, *J. Phys. Chem. B* **2008**, *112*, 15529.
20 R. Righini, *Science* **1993**, *262*, 1386.
21 A. Sengupta, M. D. Fayer, *J. Chem. Phys.* **1995**, *102*, 4193.
22 H. Shirota, *J. Phys. Chem. B* **2005**, *109*, 7053.
23 A. Sengupta, M. Terazima, M. D. Fayer, *J. Phys. Chem.* **1992**, *96*, 8619.
24 H. Shirota, E. W. Castner, Jr., *J. Am. Chem. Soc.* **2001**, *123*, 12877.
25 H. Shirota, E. W. Castner, Jr., *J. Chem. Phys.* **2006**, *125*, 034904.
26 H. Shirota, H. Ushiyama, *J. Phys. Chem. B* **2008**, *112*, 13542.
27 N. T. Hunt, A. A. Jaye, A. Hellman, S. R. Meech, *J. Phys. Chem. B* **2004**, *108*, 100.
28 N. T. Hunt, A. A. Jaye, S. R. Meech, *J. Phys. Chem. B* **2003**, *107*, 3405.
29 A. A. Jaye, N. T. Hunt, S. R. Meech, *Langmuir* **2005**, *21*, 1238.
30 R. A. Farrer, J. T. Fourkas, *Acc. Chem. Res.* **2003**, *36*, 605, and reference therein.
31 X. Zhu, R. A. Farrer, J. T. Fourkas, *J. Phys. Chem. B* **2005**, *109*, 12724.
32 J. D. Eaves, C. J. Fecko, A. L. Stevens, P. Peng, A. Tokmakoff, *Chem. Phys. Lett.* **2003**, *376*, 20.
33 G. Giraud, K. Wynne, *J. Am. Chem. Soc.* **2002**, *124*, 12110.
34 G. Giraud, J. Karolin, K. Wynne, *Biophys. J.* **2003**, *85*, 1903.
35 N. T. Hunt, L. Kattner, R. P. Shanks, K. Wynne, *J. Am. Chem. Soc.* **2007**, *129*, 3168.
36 E. W. Castner, Jr., J. F. Wishart, H. Shirota, *Acc. Chem. Res.* **2007**, *40*, 1217, and reference therein.
37 H. Shirota, K. Nishikawa, T. Ishida, *J. Phys. Chem. B* **2009**, *113*, 9831.
38 D. Xiao, L. G. Hines, Jr., S. Li, R. A. Bartsch, E. L. Quitevis, O. Russina, A. Triolo, *J. Phys. Chem. B* **2009**, *113*, 6426.
39 K. Kiyohara, Y. Kimura, Y. Takebayashi, N. Hirota, K. Ohta, *J. Chem. Phys.* **2002**, *117*, 9867.
40 N. T. Hunt, A. A. Jaye, S. R. Meech, *Phys. Chem. Chem. Phys.* **2007**, *9*, 2167.
41 D. F. Underwood, D. A. Blank, *J. Phys. Chem. A* **2003**, *107*, 956.
42 S. J. Schmidtke, D. F. Underwood, D. A. Blank, *J. Am. Chem. Soc.* **2004**, *126*, 8620.
43 S. Park, B. N. Flanders, X. Shang, R. A. Westervelt, J. Kim, N. F. Scherer, *J. Chem. Phys.* **2003**, *118*, 3917.
44 A. M. Moran, R. A. Nome, N. F. Scherer, *J. Chem. Phys.* **2007**, *127*, 184505.
45 W. T. Lotshaw, D. McMorrow, C. Kalpouzos, G. A. Kenney-Wallace, *Chem. Phys. Lett.* **1987**, *136*, 323.
46 D. McMorrow, W. T. Lotshaw, G. A. Kenney-Wallace, *Chem. Phys. Lett.* **1988**, *145*, 309.
47 D. McMorrow, W. T. Lotshaw, *J. Phys. Chem.* **1991**, *95*, 10395.
48 D. McMorrow, N. Thantu, J. S. Melinger, S. K. Kim, W. T. Lotshaw, *J. Phys. Chem.* **1996**, *100*, 10389.
49 S. Palese, S. Mukamel, R. J. D. Miller, W. T. Lotshaw, *J. Phys. Chem.* **1996**, *100*, 10380.
50 D. McMorrow, N. Thantu, V. Kleiman, J. S. Melinger, W. T. Lotshaw, *J. Phys. Chem. A* **2001**, *105*, 7960.
51 Y. J. Chang, E. W. Castner, Jr., *J. Chem. Phys.* **1993**, *99*, 113.
52 Y. J. Chang, E. W. Castner, Jr., *J. Phys. Chem.* **1994**, *98*, 9712.
53 E. W. Castner, Jr., Y. J. Chang, J. S. Melinger, D. McMorrow, *J. Lumin.* **1994**, *60–61*, 723.
54 Y. J. Chang, E. W. Castner, Jr., *J. Phys. Chem.* **1996**, *100*, 3330.
55 P. P. Wiewiór, H. Shirota, E. W. Castner, Jr., *J. Chem. Phys.* **2002**, *116*, 4643.
56 N. A. Smith, S. J. Lin, S. R. Meech, K. Yoshihara, *J. Phys. Chem. A* **1997**, *101*, 3641.
57 N. A. Smith, S. J. Lin, S. R. Meech, H. Shirota, K. Yoshihara, *J. Phys. Chem. A* **1997**, *101*, 9578.
58 N. A. Smith, S. R. Meech, *J. Phys. Chem. A* **2000**, *104*, 4223.
59 H. Shirota, *J. Chem. Phys.* **2005**, *122*, 044514.
60 H. P. Deuel, P. Cong, J. D. Simon, *J. Phys. Chem.* **1994**, *98*, 12600.
61 H. P. Deuel, P. Cong, J. D. Simon, *J. Raman Spectrosc.*

1995, *26*, 523.
62 P. Cong, H. P. Deuel, J. D. Simon, *Chem. Phys. Lett.* **1995**, *240*, 72.
63 P. Cong, J. D. Simon, C. Y. She, *J. Chem. Phys.* **1996**, *104*, 962.
64 P. Vöhringer, D. C. Arnett, R. A. Westervelt, M. J. Feldstein, N. F. Scherer, *J. Chem. Phys.* **1995**, *102*, 4027.
65 S. Kinoshita, Y. Kai, M. Yamaguchi, T. Yagi, *Phys. Rev. Lett.* **1995**, *75*, 148.
66 S. Kinoshita, Y. Kai, Y. Watanabe, *Chem. Phys. Lett.* **1999**, *301*, 183.
67 J. Watanabe, E. Ohtsuka, S. Kinoshita, *Chem. Phys. Lett.* **2002**, *361*, 259.
68 K. Kamada, M. Ueda, T. Sakaguchi, K. Ohta, T. Fukumi, *Chem. Phys. Lett.* **1996**, *249*, 329.
69 K. Kiyohara, K. Kamada, K. Ohta, *J. Chem. Phys.* **2000**, *112*, 6338.
70 R. A. Farrer, B. J. Loughnane, L. A. Deschenes, J. T. Fourkas, *J. Chem. Phys.* **1997**, *106*, 6901.
71 B. J. Loughnane, A. Scodinu, R. A. Farrer, J. T. Fourkas, U. Mohanty, *J. Chem. Phys.* **1999**, *111*, 2686.
72 A. Scodinu, J. T. Fourkas, *J. Phys. Chem. B* **2003**, *107*, 44.
73 B. J. Loughnane, A. Scodinu, J. T. Fourkas, *J. Phys. Chem. B* **2006**, *110*, 5708.
74 Q. Zhong, J. T. Fourkas, *J. Phys. Chem. B* **2008**, *112*, 15342.
75 Q. Zhong, J. T. Fourkas, *J. Phys. Chem. B* **2008**, *112*, 8656.
76 M. Ricci, P. Bartolini, R. Chelli, G. Cardini, S. Califano, R. Righini, *Phys. Chem. Chem. Phys.* **2001**, *3*, 2795.
77 A. Idrissi, M. Ricci, P. Bartolini, R. Righini, *J. Chem. Phys.* **1999**, *111*, 4148.
78 P. Foggi, P. Bartolini, M. Bellini, M. G. Giorgini, A. Morresi, P. Sassi, R. S. Cataliotti, *Eur. Phys. J. D* **2002**, *21*, 143.
79 M. Neelakandan, D. Pant, E. L. Quitevis, *Chem. Phys. Lett.* **1997**, *265*, 283.
80 M. Neelakandan, D. Pant, E. L. Quitevis, *J. Phys. Chem. A* **1997**, *101*, 2936.
81 T. F. Laurent, H. Hennig, N. P. Ernsting, S. A. Kovalenko, *Phys. Chem. Chem. Phys.* **2000**, *2*, 2691.
82 M. Khalil, O. Golonzka, N. Demirdöven, C. J. Fecko, A. Tokmakoff, *Chem. Phys. Lett.* **2000**, *321*, 231.
83 C. J. Fecko, J. D. Eaves, A. Tokmakoff, *J. Chem. Phys.* **2002**, *117*, 1139.
84 A. D. Becke, *J. Chem. Phys.* **1993**, *98*, 5648.
85 C. Lee, W. Yang, R. G. Parr, *Phys. Rev. B* **1988**, *37*, 785.
86 T. H. Dunning, Jr., *J. Chem. Phys.* **1989**, *90*, 1007.
87 D. E. Woon, T. H. Dunning, Jr., *J. Chem. Phys.* **1993**, *98*, 1358.
88 M. J. Frisch, G. W. Trucks, H. B. Schlegel, G. E. Scuseria, M. A. Robb, J. R. Cheeseman, J. A. Montgomery, Jr., T. Vreven, K. N. Kudin, J. C. Burant, J. M. Millam, S. S. Iyengar, J. Tomasi, V. Barone, B. Mennucci, M. Cossi, G. Scalmani, N. Rega, G. A. Petersson, H. Nakatsuji, M. Hada, M. Ehara, K. Toyota, R. Fukuda, J. Hasegawa, M. Ishida, T. Nakajima, Y. Honda, O. Kitao, H. Nakai, M. Klene, X. Li, J. E. Knox, H. P. Hratchian, J. B. Cross, C. Adamo, J. Jaramillo, R. Gomperts, R. E. Stratmann, O. Yazyev, A. J. Austin, R. Cammi, C. Pomelli, J. W. Ochterski, P. Y. Ayala, K. Morokuma, G. A. Voth, P. Salvador, J. J. Dannenberg, V. G. Zakrzewski, S. Dapprich, A. D. Daniels, M. C. Strain, O. Farkas, D. K. Malick, A. D. Rabuck, K. Raghavachari, J. B. Foresman, J. V. Ortiz, Q. Cui, A. G. Baboul, S. Clifford, J. Cioslowski, B. B. Stefanov, G. Liu, A. Liashenko, P. Piskorz, I. Komaromi, R. L. Martin, D. J. Fox, T. Keith, M. A. Al-Laham, C. Y. Peng, A. Nanayakkara, M. Challacombe, P. M. W. Gill, B. Johnson, W. Chen, M. W. Wong, C. Gonzalez, J. A. Pople, *Gaussian 03, Revision B.03,* Gaussian Inc., Pittsburgh PA, **2003**.
89 D. A. Long, *The Raman Effect*, John Wiley & Sons, West Sussex, **2002**.
90 M. Le Guennec, K. Evain, B. Illien, *THEOCHEM* **2001**, *542*, 167.
91 D. McMorrow, W. T. Lotshaw, *Chem. Phys. Lett.* **1990**, *174*, 85.
92 H. Cang, J. Li, V. N. Novikov, M. D. Fayer, *J. Chem. Phys.* **2003**, *118*, 9303.
93 H. Cang, V. N. Novikov, M. D. Fayer, *Phys. Rev. Lett.* **2003**, *90*, 197401.
94 J. Li, H. Cang, H. C. Andersen, M. D. Fayer, *J. Chem. Phys.* **2006**, *124*, 014902.
95 M. Cho, M. Du, N. F. Scherer, G. R. Fleming, S. Mukamel, *J. Chem. Phys.* **1993**, *99*, 2410.
96 H. Shirota, K. Yoshihara, N. A. Smith, S. J. Lin, S. R. Meech, *Chem. Phys. Lett.* **1997**, *281*, 27.
97 Y. J. Chang, E. W. Castner, Jr., *J. Chem. Phys.* **1993**, *99*, 7289.
98 N. A. Smith, S. R. Meech, *Faraday Discuss.* **1997**, *108*, 35.
99 J. R. Rajian, B.-R. Hyun, E. L. Quitevis, *J. Phys. Chem. A* **2004**, *108*, 10107.
100 P. Bartolini, M. Ricci, R. Torre, R. Righini, I. Sánta, *J. Chem. Phys.* **1999**, *110*, 8653.
101 H. Shirota, E. W. Castner, Jr., *J. Phys. Chem. B* **2005**, *109*, 21576.
102 H. Shirota, J. F. Wishart, E. W. Castner, Jr., *J. Phys. Chem. B* **2007**, *111*, 4819.
103 B.-R. Hyun, S. V. Dzyuba, R. A. Bartsch, E. L. Quitevis, *J. Phys. Chem. A* **2002**, *106*, 7579.
104 D. Xiao, J. R. Rajian, A. Cady, S. Li, R. A. Bartsch, E. L. Quitevis, *J. Phys. Chem. B* **2007**, *111*, 4669.
105 S. Mukamel, *Principles of Nonlinear Optical Spectroscopy*, Oxford University Press, New York, **1995**.
106 Y. Tanimura, S. Mukamel, *J. Chem. Phys.* **1993**, *99*, 9496.
107 Y. Nagata, T. Hasegawa, Y. Tanimura, *J. Chem. Phys.* **2006**, *124*, 194504.
108 *CRC Handbook of Chemistry and Physics*, 89th ed., ed. by D. R. Lide, CRC Press, Boca Raton, **2008**.
109 T. Zamir, T. I. Quickenden, *J. Solution Chem.* **2003**, *32*, 463.
110 M. G. Freire, A. G. M. Ferreira, I. M. A. Fonseca, I. M. Marrucho, J. A. P. Coutinho, *J. Chem. Eng. Data* **2008**, *53*, 538.
111 R. Freer, J. N. Sherwood, *J. Phys. Chem.* **1981**, *85*, 102.
112 J. T. Edward, *J. Chem. Educ.* **1970**, *47*, 261.
113 A. Bondi, *J. Phys. Chem.* **1964**, *68*, 441.
114 D. A. McQuarrie, J. D. Simon, *Physical Chemistry: A Molecular Approach*, University Science Books, Sausalito, **1997**.
115 S. Iuchi, A. Morita, S. Kato, *J. Phys. Chem. B* **2002**, *106*, 3466.
116 T. Ishida, A. Morita, *J. Chem. Phys.* **2006**, *125*, 074112.
117 M. J. Earle, J. M. S. S. Esperança, M. A. Gilea, J. N. C. Lopes, L. P. N. Rebelo, J. W. Magee, K. R. Seddon, J. A. Widegren, *Nature* **2006**, *439*, 831.
118 M. S. Skaf, S. M. Vechi, *J. Chem. Phys.* **2003**, *119*, 2181.
119 S. Ryu, R. M. Stratt, *J. Phys. Chem. B* **2004**, *108*, 6782.
120 M. D. Elola, B. M. Ladanyi, *J. Chem. Phys.* **2007**, *126*, 084504.
121 R. Kubo, *A Stochastic Theory of Line-Shape and*

Relaxation in *Fluctuation, Relaxation and Resonance in Magnetic Systems*, ed. by D. T. Haar, Oliver and Boyd, Edinburgh, **1961**, p. 23.
122 G. Tao, R. M. Stratt, *J. Phys. Chem. B* **2006**, *110*, 976.
123 M. D. Elola, B. M. Ladanyi, *J. Phys. Chem. B* **2006**, *110*, 15525.
124 A. A. Jaye, N. T. Hunt, S. R. Meech, *J. Chem. Phys.* **2006**, *124*, 024506.
125 J. N. Israelachvili, *Intermolecular and Surface Forces*, 2nd ed., Academic Press, London, **1992**.
126 A. J. Stone, *The Theory of Intermolecular Forces*, Clarendon Press, Oxford, **1996**.
127 H. Jin, B. O'Hare, J. Dong, S. Arzhantsev, G. A. Baker, J. F. Wishart, A. J. Benesi, M. Maroncelli, *J. Phys. Chem. B* **2008**, *112*, 81.
128 H. Shirota, E. W. Castner, Jr., *J. Phys. Chem. A* **2005**, *109*, 9388.
129 D. Kivelson, P. A. Madden, *Annu. Rev. Phys. Chem.* **1980**, *31*, 523.
130 J. L. Dote, D. Kivelson, R. N. Schwartz, *J. Phys. Chem.* **1981**, *85*, 2169.
131 G. R. Fleming, *Chemical Applications of Ultrafast Spectroscopy*, Oxford University Press, New York, **1986**.
132 D. A. Turton, K. Wynne, *J. Chem. Phys.* **2008**, *128*, 154516.
133 R. T. Boeré, R. G. Kidd, *Annu. Rep. NMR Spectrosc.* **1983**, *13*, 319.
134 D. Ben-Amotz, J. M. Drake, *J. Chem. Phys.* **1988**, *89*, 1019.
135 M. Roy, S. Doraiswamy, *J. Chem. Phys.* **1993**, *98*, 3213.